Title: Bile salt hydrolases deplete conjugated bile acids and erode gut barrier integrity in non-alcoholic steatohepatitis

Short Title: Conjugated bile acids in NASH

Authors: Darrick K. Li[1†*], Snehal N. Chaudhari[2†], Mozhdeh Sojoodi[3], Yoojin Lee[1], Arijit A. Adhikari[2], Zhu Zhuo[4], Lawrence Zukerberg[5], Stuti Shroff[5], Stephen Cole Barrett[3], Jerome Boursier[6], Anna Mae Diehl[7], Shannan Ho Sui[4], Kenneth Tanabe[3], Raymond T. Chung[1**], A. Sloan Devlin[2**]

[1]Liver Center, Massachusetts General Hospital, Harvard Medical School, Boston, MA, USA

[2]Department of Biological Chemistry and Molecular Pharmacology, Blavatnik Institute, Harvard Medical School, Boston, MA, USA

[3]Department of Surgery, Massachusetts General Hospital, Harvard Medical School, Boston, MA, USA

[4]Harvard Chan Bioinformatics Core, Department of Biostatistics, Harvard T.H. Chan School of Public Health, Boston, MA, USA

[5]Department of Pathology, Massachusetts General Hospital, Harvard Medical School, Boston, MA, USA

[6]Service d'Hépato-Gastroentérologie, Centre Hospitalier Universitaire d'Angers, Angers, France; & Laboratoire HIFIH UPRES EA3859, Université d'Angers, Angers, France

[7]Division of Gastroenterology, Department of Medicine, Duke University Medical Center, Durham, NC, USA

† Co-first author

* Current address: Section of Digestive Diseases, Department of Medicine, Yale School of Medicine, New Haven, CT, USA

Grant Support: The research was supported by National Institutes of Health (NIH) grant R35 GM128618 (A.S.D.), an Innovation Award from the Center for Microbiome Informatics and

Therapeutics at MIT (A.S.D), a grant from Harvard Digestive Diseases Center (supported by NIH grant 5P30DK034854-32) (A.S.D), a John and Virginia Kaneb Fellowship (A.S.D), a Quadrangle Fund for the Advancement and Seeding of Translational Research at Harvard Medical School (Q-FASTR) grant (A.S.D), an HMS Dean's Innovation Grant in the Basic and Social Sciences (A.S.D), and the MGH Research Scholars Program (R.T.C.). D.K.L. was supported by National Institutes of Health T32 training grant (5T32DK007191). S.N.C. acknowledges an American Heart Association Postdoctoral Fellowship. Work by Z.Z. and S.H.S. was funded in part by the Harvard Medical School Foundry.

Abbreviations: α/βMCA = α/β-muricholic acid, ALT = alanine aminotransferase; AST = aspartate aminotransferase; BA = bile acid, BSH = bile salt hydrolase; CA = cholic acid; CA7S = cholic acid-7-sulfate; CDAHFD = choline-deficient, L-amino acid defined, high-fat diet; CDCA = chenodeoxycholic acid; CDCA-d4 = deuterated chenodeoxycholic acid; CMC = critical micellar concentration; DCA = deoxycholic acid; FXR = farnesoid X receptor; GCDCA-d4 = deuterated glycochenodeoxycholic acid; LPS = lipopolysaccharide; NAFLD/NASH = non-alcoholic fatty liver disease/non-alcoholic steatohepatitis; SEM = standard error of the mean; Tα/βMCA = tauro-α/β-muricholic acid; TCA = tauro-cholic acid; TCDCA = tauro-chenodeoxycholic acid; TDCA = tauro-deoxycholic acid; TEM = transmission electron microscopy; TUDCA = tauro-ursodeoxycholic acid; UDCA = ursodeoxycholic acid; UPLC-MS = ultra-high performance liquid chromatography-mass spectrometry

****Correspondence:**

Raymond T. Chung: 55 Fruit Street, Boston, MA 02114; Warren Building Room 1007C; Telephone: 617-726-5925; Fax: 617-724-6832; E-mail: Chung.Raymond@mgh.harvard.edu

A. Sloan Devlin: 250 Longwood Ave, Boston, MA 02115; Seeley G. Mudd Building Room 622B; Telephone: 617-432-5186; E-mail: sloan_devlin@hms.harvard.edu

Disclosures: The authors declare the following competing financial interest(s): A.S.D. is an *ad hoc* consultant for Takeda Pharmaceuticals and HP Hood. The other authors declare that no competing interests exist.

Transcript Profiling: None.

Writing Assistance: No assistance was used in the writing of this manuscript.

Author Contributions: D.K.L., S.N.C., R.T.C, and A.S.D. conceived the project and designed the experiments. D.K.L., M.S., Y.L, and S.C.B. performed all animal experiments, immunofluorescence, staining, and transcriptional analyses on rat tissues. S.N.C. performed the cell culture experiments, BA profiling, and preparation for electron microscopy. Z.Z. and S.H.S. performed statistical analysis on human bile acid data. S.S. and L.Z. performed pathology scoring of rat tissue. J.B. and A.M.D. collected and provided the human samples. D.K.L., S.N.C., and A.S.D. wrote the manuscript. All authors edited and contributed to the critical review of the manuscript.

Data Transparency Statement: All data generated or analyzed during this study are included in this article and its Supplementary Information.

Acknowledgements: We are indebted to members of the Devlin, Chung, and Tanabe groups for helpful discussions. We thank the HMS Electron Microscopy core for technical support and advice. We are grateful to the human patients who participated in this study.

Abstract

Background & Aims: While altered host-microbe interactions are implicated in non-alcoholic fatty liver disease/non-alcoholic steatohepatitis (NAFLD/NASH), specific contributions of microbially derived metabolites remain obscure. We investigated the impact of altered bile acid (BA) populations on intestinal and hepatic phenotypes in a rodent model of NAFLD/NASH.

Methods: Wistar rats fed a choline-deficient high-fat diet (CDAHFD) were assessed for altered intestinal permeability after dietary intervention. Cecal and portal venous BA composition were assessed via mass spectrometry. BA-mediated effects on epithelial permeability were assessed using Caco2 epithelial monolayers. Micelle formation was assessed using fluorescent probes and electron microscopy. Bile salt hydrolase (BSH) activity was inhibited with a gut-restricted small molecule in CDAHFD-fed rats and intestinal and hepatic phenotypes were assessed.

Results: Increased intestinal permeability and reduced intestinal conjugated BAs were early phenotypes of CDAHFD-fed rats preceding hepatic disease development. Similar intestinal BA pool changes were observed in rats and human NAFLD/NASH patients with progressive disease. Conjugated BAs protected epithelial layers from unconjugated BA-induced damage via mixed micelle formation. The decrease in intestinal conjugated BAs was mediated by increased activity of bacterial BSHs and inhibition of BSH activity prevented the development of pathologic intestinal permeability and hepatic inflammation in the NAFLD/NASH model.

Conclusions: Conjugated BAs are important for the maintenance of intestinal barrier function by sequestering unconjugated BAs in mixed micelles. Increased BSH activity reduces intestinal conjugated BA abundance, in turn increasing intestinal permeability and susceptibility to the development of NAFLD/NASH. These findings suggest that interventions that shift the intestinal bile acid pool toward conjugated BAs could be developed as therapies for NAFLD/NASH.

Keywords: Bile Salt Hydrolase; Conjugated Bile Acid; Intestinal Permeability; Non-alcoholic steatohepatitis; Mixed Micelles

What You Need To Know

BACKGROUND AND CONTEXT: Altered host-microbe interactions are implicated in the development of NAFLD/NASH but the contributions of specific microbially derived metabolites have remained obscure.

NEW FINDINGS: Conjugated BAs protect intestinal epithelium by sequestering unconjugated BAs in mixed micelles. Reduced intestinal conjugated BAs resulting from increased bacterial BSH activity is observed in a rodent model of NAFLD/NASH. BSH inhibition leads to improved intestinal and hepatic phenotypes.

LIMITATIONS: This study was performed primarily in rats with supportive human fecal BA data. Additional studies are required to further support the relevance of our findings in human disease.

IMPACT: Conjugated BAs and bacterial BSH activity are important for intestinal barrier function in NAFLD/NASH. Interventions shifting the intestinal BA pool toward conjugated BAs may be developed as therapies for NAFLD/NASH.

Short Summary: Inhibition of bile salt hydrolase activity and increased intestinal conjugated bile acids protect against early damage to intestinal barrier integrity and hepatic inflammation in a rodent model of non-alcoholic steatohepatitis.

Introduction

Gut microbial imbalance has been proposed to contribute to the development of chronic liver disease, including non-alcoholic fatty liver disease/non-alcoholic steatohepatitis (NAFLD/NASH), conditions which affect nearly 25% of the global population[1, 2]. Though gut dysbiosis is a central feature of human NAFLD/NASH[3, 4], the mechanistic links between specific alterations in microbial metabolic output and disease development remain largely uncharacterized.

Emerging data have implicated increased intestinal permeability as an early feature of NAFLD/NASH that may contribute directly to the development of liver injury[5-8]. A recent meta-analysis demonstrated that NAFLD and NASH patients had a significantly increased prevalence of intestinal permeability compared to healthy controls[5]. In health, the intestinal epithelium forms a dynamic and tightly sealed barrier that is selectively permeable[9]. However, under pathologic conditions, tight junction proteins can become disrupted with excessive leakage of dietary and bacterial antigens, including lipopolysaccharide (LPS), into the portal and systemic circulation, directly inducing hepatic inflammation[10]. Changes in intestinal microbiome composition in NAFLD/NASH patients have been hypothesized to contribute to the development of pathologic intestinal permeability[11]. However, specific host and microbial factors that result in the development of pathologic intestinal permeability remain unclear.

Bile acids (BAs) are a class of microbially modified metabolites that have been implicated as potential causal agents in the pathophysiology of NAFLD/NASH[12-14]. BAs are steroidal products synthesized from cholesterol in the liver and are present in high concentrations in the intestine. These compounds are conjugated to either taurine or glycine by host liver enzymes and are hydrolyzed by bacterial bile salt hydrolases (BSHs) in the intestine to produce unconjugated bile acids[15]. BSHs are bacterially encoded enzymes and have no mammalian homolog[16]. BSH activity is critical to BA metabolism in the gut; deconjugation is required before further bacterial

149 modifications, including 7α-dehydroxylation and epimerization, can be performed to produce
150 secondary BAs. BSHs are expressed in a broad range of human gut bacteria[17].
151
152 While changes in serum BA profiles have been reported to correlate with disease severity in
153 NAFLD/NASH patients, the mechanistic contribution of specific BA populations to the
154 pathogenesis of disease has not been well elucidated[12-14]. Previous work has demonstrated that
155 exposure of epithelial monolayers to certain hydrophobic BAs, including unconjugated BAs, leads
156 to increased intestinal permeability *in vitro* and may contribute to the development of intestinal
157 inflammation and disruption of intestinal homeostasis *in vivo*[18, 19]. In animal models, long-term
158 administration of a high-fat diet in mice has recently been shown to lead to increased intestinal
159 permeability associated with an enrichment of hydrophobic BAs in the intestinal BA pool[20-22].
160 These findings prompted us to investigate how changes in intestinal BA populations contribute to
161 the development of pathologic intestinal permeability.
162
163 Here, we demonstrate that increased intestinal permeability is an early feature of a rat model of
164 NAFLD/NASH that precedes the development of hepatic injury and that changes in cecal BA
165 profiles that occur with disease progression in the animal model closely resemble changes in fecal
166 BA profiles in humans with NAFLD/NASH. We also show that at early timepoints, there is a
167 significant reduction in the amount of intestinal conjugated BAs in diseased rats. In addition, we
168 demonstrate that conjugated BAs sequester unconjugated BAs into mixed micelles and protect
169 epithelial cells from damage and permeability. Furthermore, we identify increased bacterial BSH
170 activity as a driver of decreased cecal conjugated BAs and that inhibition of bacterial BSH
171 prevents the development of increased intestinal permeability and attenuates hepatic steatosis
172 and inflammation in diseased rats.

Materials and Methods

A detailed description of the Materials and Methods can be found in the Supplementary Material.

Animals. 8-week old Wistar rats were purchased from Charles River Laboratories (Wilmington, MA) and housed in a specific pathogen-free environment (maximum four per cage). After 10 days of acclimation, rats were initiated on either a control high-fat diet (60 kcal% fat; Research Diets D12492) or CDAHFD (L-amino acid diet with 60 kcal% fat with 0.1% methionine without added choline; Research Diets A06071302) *ad libitum* for either 48 hours or 1 week (either 7 or 8 days). At time of sacrifice, rats were anesthetized using 100 mg/kg of ketamine and 10 mg/kg of xylazine intraperitoneally followed by portal vein blood draw and terminal cardiac puncture.

Ethics. Animals received humane care per criteria outlined in the Guide for the Care and Use of Laboratory Animals by the National Academy of Sciences (National Institutes of Health publication 86-23, revised 1985) and in accordance with the Massachusetts General Hospital Institutional Animal Care and Use Committee guidelines (Protocol 2007N000113). The human study protocol conformed to the ethical guidelines of the current Declaration of Helsinki and was approved by the local ethics committee (Massachusetts General Hospital IRB 2020P002446). All patients gave informed written consent before participating to the study.

AAA-10 treatment. After initiation of CDAHFD diet, rats were split into two groups and were gavaged twice a day with either 10 mg/kg of AAA-10 dissolved in 5% Captisol (Ligand, San Diego, CA) and 10% DMSO in PBS or an equal volume of 5% Captisol and 10% DMSO in PBS.

***In vitro* bile acid treatments**. Caco-2 cells (undifferentiated in 96-well plates or day 21 to 25 of differentiation in transwells) were treated with bile acid mixtures for 12-16 hours prior to assays. Diluted stocks of bile acid standards or undiluted methanol-extracted cecal contents were added

199 in complete media. Transcytosis of bile acids was measured by drying basolateral media in a
200 speed vac followed by resuspending media in 1:1 methanol/water, transferred into mass
201 spectrometry vials and injected onto the ultra-high performance liquid chromatography-mass
202 spectrometer (UPLC-MS).
203
204 **Caco-2 permeability assay**. Epithelial integrity by FITC-dextran permeability assay was
205 performed as described previously[23]. Briefly, differentiated Caco-2 epithelial integrity was assayed
206 by measuring passive diffusion of 4 kDa FITC-Dextran (Sigma Aldrich) added at a concentration
207 of 5 μM to the apical chamber in 100 μL PBS, while the basolateral chamber contained 500 μL
208 PBS. Diffusion from the apical to basolateral side was measured by fluorescence reading in PBS
209 on the basolateral side of the transwell system using a SpectraMax M5 plate reader (Molecular
210 Devices, San Jose, CA) at the ICCB-Longwood Screening Facility. Fluorescence reading was
211 normalized to the control.
212
213 **Critical micelle concentration (CMC) assay**. CMC determination of groups of bile acids was
214 performed using a previously described assay using coumarin 6 as a fluorescent probe with minor
215 adaptations[24]. 6 mM coumarin 6 (Sigma) in dichloromethane (Sigma) was added to Eppendorf
216 tubes and allowed to evaporate for 30 min in a chemical hood. 400 μL of equimolar mixtures of
217 bile acids at various concentrations to be tested were added to tubes and rotated overnight at
218 room temperature in the dark (unconjugated BAs: beta-muricholic acid [βMCA], cholic acid [CA],
219 deoxycholic acid [DCA], ursodeoxycholic acid [UDCA], chenodeoxycholic acid [CDCA]);
220 conjugated BAs: tauro-beta-muricholic acid [TβMCA], tauro-cholic acid [TCA], tauro-deoxycholic
221 acid [TDCA], tauro-ursodeoxycholic acid [TUDCA], tauro-chenodeoxycholic acid [TCDCA]). The
222 next day, 200 μL of the solution was transferred to black 96 well plates (Costar), and fluorescence
223 intensity at 480/530 was measured using a SpectraMax M5 plate reader (Molecular Devices, San
224 Jose, CA) at the ICCB-Longwood Screening Facility. Fluorescence intensity was plotted against

the logarithm of the corresponding concentration and the CMC was determined by the intersection of the two tangents created in the graph.

BSH activity assay. BSH activity was quantified using a modified version of a previously described method[25]. Briefly, fresh cecal contents (approximately 20 mg) were diluted in PBS to obtain a concentration of 1 mg/mL 100 µM glycochenodeoxycholic acid-d4 (GCDCA-d4) was added to the mixture and incubated at 37ºC for 30 minutes, then frozen in dry ice for 5 minutes and stored at -80ºC until further analysis. On thawing, the mixture was diluted with an equal volume of methanol and the slurry was centrifuged at 12,500 x g for 10 minutes. The supernatant was removed into a clean Eppendorf tube and centrifuged again. The supernatant was transferred to mass spectrometry vials and samples were analyzed as described in Bile Acid Analysis in Supplementary Information.

Statistical Analyses. Data was quantified using software linked to indicated instruments and plotted in GraphPad Prism 7. Statistical analyses were performed using GraphPad Prism and Microsoft Excel software. Statistical significance was assessed using Student's or Welch's t tests, one-way or two-way ANOVAs followed by multiple comparisons tests, and Mann-Whitney tests wherever appropriate. For clinical characteristics, quantitative variables were expressed as median and interquartile range. Discrete variables were compared using the Fischer's exact test or chi-squared test where appropriate and continuous variables were compared using the unpaired student's *t*-test. Further details are described in Supplementary Information.

Results

CDAHFD-fed rats develop increased intestinal permeability prior to developing hepatic inflammation

To begin investigating the molecular mechanisms leading to the development of intestinal permeability in NAFLD/NASH, we utilized an established rodent model of diet-induced cirrhosis using a choline-deficient, L-amino acid defined, high-fat diet (CDAHFD). Consistent with previous reports, CDAHFD-fed rats developed cirrhosis in 12 weeks[26] while controls fed a high-fat diet with equivalent fat by weight developed microvesicular steatosis without inflammation or fibrosis (**Figure S1A**). CDAHFD-fed rats gained less weight than controls and exhibited significantly increased markers of hepatocellular injury, hepatic hydroxyproline levels, and mRNA expression of fibrosis-related and inflammatory genes at 12 weeks post-diet intervention (**Figure 1A, S1B-D**). To assess intestinal permeability, we measured portal venous bile acid levels and LPS in cirrhotic rats. LPS levels were significantly higher in CDAHFD-fed rats compared to controls at 12 weeks (**Figure S1E**). Furthermore, UPLC-MS-based BA profiling revealed detectable levels of cholic acid-7-sulfate (CA7S), a gut-restricted BA[23, 27], in the portal vein of CDAHFD-fed rats, while no detectable portal venous CA7S was detected in control rats (**Figure S1F**). These findings indicate that CDAHFD-fed rats develop cirrhosis and increased intestinal permeability within 12 weeks of diet initiation.

To investigate whether intestinal permeability was present at early timepoints, we measured portal LPS levels at 48 hours and 1 week post-CDAHFD, when biochemical markers of liver injury were not significantly elevated (**Figure 1A**). Remarkably, LPS levels were higher in CDAHFD-fed rats compared to controls as early as 48 hours post-diet intervention (**Figure 1B**). Intestinal epithelium from CDAHFD-fed rats exhibited significantly increased inflammation and epithelial hyperplasia at early time points when serum biomarkers of liver injury were not significantly elevated (**Figure 1C**). Expression of tight junction genes including *Zo-1*, *occludin*, and *Claudin1* were not

significantly different between CDAHFD-fed and control rats at early timepoints (**Figure S2**). However, we observed significantly increased membrane localization of ZO-1 in intestinal epithelial cells of CDAHFD-fed rats at 48 hours that persisted after 1 week of diet (**Figure 1D**). Increased expression and plasma membrane localization of ZO-1 are indicative of increased intestinal permeability[28]. Moreover, treatment of gut epithelial cells with permeability agents results in dynamic changes in ZO-1 subcellular localization, including recruitment to the plasma membrane[29, 30]. As such, ZO-1 redistribution in the intestinal epithelium of CDAHFD-fed rats is consistent with increased intestinal permeability. To confirm these results, using a FITC-Dextran assay, we found that CDAHFD-fed rats exhibited a significant increase in intestinal permeability compared to controls at 48 hours after diet initiation (**Figure 1E**). Importantly, at 48 hours, CDAHFD-fed rats did not exhibit any evidence of hepatic inflammation compared to controls while inflammation was apparent at 1 week post-dietary intervention (**Figure 1F-H**). Together, these results demonstrate that intestinal permeability is an early feature of this animal model and precedes the development of hepatic inflammation.

Cecal BA composition changes in CDAHFD-fed rats reflect fecal BA composition changes in NAFLD/NASH patients

To assess whether changes in BAs are associated with increased intestinal permeability, we performed intestinal and portal venous BA profiling in CDAHFD-fed and control rats. UPLC-MS analysis revealed a significant decrease in total cecal BAs and in unconjugated BAs in CDAHFD-fed rats at late timepoints compared to control animals (**Figure 2A,B**). Interestingly, at the same timepoints, portal venous BA profiling revealed the inverse finding, with significantly higher concentrations of total and unconjugated BAs in CDAHFD-fed rats compared to controls (**Figure 2C,D**). No significant differences were observed in the expression of genes involved in BA synthesis (*Cyp7a1, Cyp8b1,Cyp27a1*) or transport (Asbt, Osta/*Ostb*) (**Figure S3A,B**), indicating that the observed changes are unlikely to be the result of decreased BA synthesis or increased

BA transport. These findings suggest that at advanced stages of disease, CDAHFD-fed rats exhibit increased intestinal permeability resulting in intestinal BA leakage into the portal circulation.

We next sought to establish whether our BA findings in our animal model were relevant to human disease. To accomplish this goal, we characterized fecal BA profiles from an adult cohort with biopsy-proven NAFLD/NASH[3]. Given hepatic fibrosis severity is the primary histologic prognostic factor for mortality and liver-related complications in NAFLD/NASH patients[31], fecal BA concentrations were analyzed for correlations with severity of fibrosis stage. Paired liver biopsy and stool samples collected on the same day were analyzed from 62 patients with a median age of 59. Of these patients, 47 (76%) had F0-F2 fibrosis stage on liver biopsy and 15 (24%) had F3-F4 fibrosis. Overall, patients with F3-F4 fibrosis had significantly higher prevalence of diabetes mellitus (73% vs. 40%) and significantly higher serum GGT and AST levels (**Table 1**). Similar to CDAHFD-fed rats, we observed significantly decreased total and unconjugated BAs in patients with more severe disease (**Figure 2E,F**). Thus, human fecal BA profiles mirrored changes observed in CDAHFD-fed rats as disease progressed, suggesting that our animal model data reflects relevant disease-related alterations in NAFLD/NASH.

Conjugated BAs are reduced in the cecum of CDAHFD-fed rats at early timepoints

We reasoned that altered intestinal BA profiles contribute to the development of increased intestinal permeability observed at early timepoints in CDAHFD-fed rats. To assess this hypothesis, we quantified cecal BAs at 48 hours and 1 week after diet change. We observed a significant decrease in the abundance of cecal and portal venous conjugated BAs in CDAHFD-fed rats at both timepoints (**Figure 2G-H**). Total cecal and portal venous BA concentrations were similar between the two groups at 48 hours and 1 week after dietary intervention (**Figure S4A**). Unconjugated BA concentrations were similar at both timepoints in the cecum, though portal

venous unconjugated BA concentration was significantly increased at 1 week (**Figure S4B**). These findings indicate that changes in cecal and portal venous BA composition precede the appearance of liver injury in CDAHFD-fed rats and suggest that loss of conjugated BAs may play a causal role in this process.

Intestinal permeability and inflammation are regulated in part by the BA-sensing farnesoid X receptor (FXR), which has been linked to NAFLD/NASH pathogenesis[32, 33]. At 48 hours after dietary intervention, ileal *Fgf15* expression was similar in both groups when multiple lines of evidence for increased intestinal permeability were already observed in CDAHFD-fed animals (**Figure S5**). After 1 week, a decrease in ileal *Fgf15* expression in CDAHFD-fed rats was observed. Our findings suggest that FXR-independent mechanisms are responsible for the earliest events that establish intestinal barrier dysfunction in this NAFLD/NASH animal model.

Conjugated BAs protect intestinal epithelium from unconjugated BA-mediated epithelial damage *in vitro*

We next hypothesized that changes in intestinal BA profiles in CDAHFD-fed rats directly contribute to increased intestinal permeability at early timepoints after dietary intervention. To test this hypothesis, we utilized differentiated Caco-2 cells in transwell inserts as an *in vitro* model system. Gut permeability was assayed by measuring FITC-Dextran (4 kDa) permeability through the monolayer and quantifying fluorescence in the basolateral chamber[23]. We found that cecal extracts isolated from CDAHFD-fed rats at early timepoints induced increased permeability compared to cecal extracts from control rats (**Figure 3A**). Similar findings were noted when assessing cecal contents from late timepoints (**Figure S6**). These findings demonstrate that intestinal contents from CDAHFD-fed rats induce epithelial barrier permeability at early timepoints.

To test whether cecal BAs specifically induce intestinal permeability in CDAHFD-fed rats, we generated reconstituted pools of BAs that mimic the average physiological concentrations observed in rat ceca and tested their ability to induce permeability in Caco2 monolayers *in vitro*. Total BAs mimicking the cecal BA profile of CDAHFD-fed rats at 48 hours post-dietary intervention induced significantly higher permeability than the DMSO control (**Figure 3B**). Interestingly, while the unconjugated BA pool alone induced a significant increase in permeability, the conjugated BA pool did not damage the monolayer barrier integrity. Remarkably, at later time points (1, 6, 12 weeks), the addition of conjugated BAs to unconjugated BAs mitigated the severity of epithelial permeability compared to unconjugated BAs alone (**Figure 3B**).

We next hypothesized that reduced cecal conjugated BAs are responsible for disruption of the epithelial integrity. To test this hypothesis, we generated equimolar pools of the predominant cecal BAs *in vivo*. We treated differentiated Caco-2 monolayers with increasing concentrations of either (1) unconjugated BAs (βMCA, CA, DCA, UDCA, CDCA); (2) conjugated BAs (TβMCA, TCA, TDCA, TUDCA, TCDCA) or (3) combined BA pools, followed by the permeability assessment (**Figure 3C**).

At physiological concentrations of BAs (~500-4000 μM), epithelial monolayer integrity was compromised after addition of unconjugated BAs but damage was prevented by addition of an equimolar concentration of conjugated BAs (**Figure 3D**). Conjugated BAs alone did not disrupt monolayer integrity at any concentrations tested. Similarly, while unconjugated BAs were toxic to cells, equimolar addition of conjugated BAs abrogated this effect (**Figure 3E**). Visualization of Caco-2 monolayers by hematoxylin and eosin staining further confirmed the toxic effects of unconjugated BAs were largely rescued by addition of conjugated BAs (**Figure 3F**). Finally, to assess the integrity of tight junctions in the epithelial monolayers, we performed transmission electron microscopy (TEM) on Caco2 monolayers exposed to the above BA groups. We identified

dilatations in the tight junctions of Caco2 cells exposed to unconjugated BAs alone not present in cells exposed to conjugated BAs alone or to a combination of both (**Figure 3G, Figure S7**). These tight junction dilatations have been observed in ileal enterocytes of Crohn's disease patients and correlate with increased permeability[34]. Together, these results demonstrate that while unconjugated BAs damage the gut epithelium, conjugated BAs protect against intestinal epithelial damage and permeability.

Conjugated BAs sequester unconjugated BAs through the formation of mixed micelles

We next sought to determine the mechanism by which conjugated BAs protect intestinal epithelial monolayers from unconjugated BA-mediated permeability. BAs are detergents and effectively solubilize fats and vitamins by forming micelles in the intestine[35]. We hypothesized that when combined, conjugated BAs form mixed micelles with unconjugated BAs, sequestering unconjugated BAs away from the epithelial cells in the gut lumen. To test this hypothesis, we assessed the critical micelle concentration (CMC) of these BA populations using a fluorescent probe[24]. Unconjugated BAs are expected to have a higher CMC compared to conjugated BAs[36]. If mixed micelles formed after combining unconjugated and conjugated BA populations, we would expect the CMC of the combined populations to be lower than that seen with unconjugated BAs alone. Consistent with this hypothesis, the combined pool CMC was 4.2 mM while the unconjugated and conjugated BA pool CMCs were 6.7 mM and 4.0 mM, respectively (**Figure 4A**). The addition of 80 mM urea prevented micelle formation as previously described (**Figure 4B**)[35]. We also performed direct visualization of micelles using negative staining-electron microscopy. At 5 mM concentration, no micelles were visualized in the unconjugated BA pool while micelles were seen in the conjugated BA pool, consistent with our CMC determinations (**Figure 4C**). Combining BA pools resulted in larger micelles indicative of mixed micelles while urea prevented formation of these micelles. Importantly, urea disrupted micelle formation without Caco2 toxicity

(**Figure 4D**). Thus, in the presence of conjugated BAs, unconjugated BAs are sequestered in mixed micelles.

To further confirm that the protective effects of conjugated BAs are micelle-dependent, we observed that addition of urea resulted in loss of conjugated BA-mediated protection of epithelial barrier integrity and cell viability (**Figure 4E-G**). Finally, we exposed Caco2 monolayers to combined BA pools in the presence or absence of urea and quantified the amount of unconjugated BAs that passed through the monolayer into the basolateral chamber by UPLC-MS. We observed significantly increased amounts of unconjugated BAs were observed in the basolateral chamber in the presence of urea, consistent with our previous observations (**Figure 4H**). Together, our data provides evidence that unconjugated BAs lead to increased permeability across an intestinal epithelial monolayer via a cytotoxic effect and that this effect is ameliorated by the addition of conjugated BAs *in vitro* via formation of mixed micelles.

BSH inhibition by AAA-10 prevents altered intestinal permeability and hepatic inflammation in CDAHFD-fed rats

We next sought to determine the etiology of the decreased conjugated BA pool *in vivo* in CDAHFD-fed rats. We hypothesized that the decrease in cecal conjugated BAs was due to increased BSH activity in the microbiome of CDAHFD-fed rats.

Using a previously described assay of *in vivo* BSH activity[25], we found that cecal BSH activity of CDAHFD-fed rats was significantly increased compared to control rats (**Figure 5A**). Importantly, no significant differences were seen in expression of BA synthesis or conjugation genes between CDAHFD-fed and control rats at 48 hours after dietary intervention (**Figure S8**). These data suggest that the decrease in conjugated BAs in CDAHFD-fed rats is driven by an increase in microbial-dependent BA deconjugation and not from decreased host BA synthesis or conjugation.

Because conjugated BAs appear to be protective against intestinal epithelial damage, we hypothesized that increased microbial BA deconjugation by BSH contributes to the development of intestinal permeability in CDAHFD-fed rats. We have previously reported the development of a covalent pan-inhibitor of gut bacterial BSHs that effectively inhibits BSH activity and increases *in vivo* levels of conjugated BAs[25]. We thus hypothesized that treatment of CDAHFD-fed rats with a gut-restricted BSH inhibitor, AAA-10, would prevent increased intestinal permeability[37]. A dose of 10 mg/kg AAA-10 or vehicle control was administered via gavage twice a day for 7 days to CDAHFD-fed rats (**Figure 5B)**. AAA-10 administration led to ~30-50 μM AAA-10 in cecal contents 48 hours and 1 week post-gavage (**Figure 5C**). No AAA-10 was detected in peripheral blood (**Figure S9A**), a finding that is consistent with our previous results[37] and indicates that this BSH inhibitor exhibits low systemic exposure. We found that AAA-10 reduced cecal BSH activity of CDAHFD-fed rats (**Figure 5D**) and significantly increased the abundance of conjugated BAs by 1 week (**Figure 5E**). We also observed significant decreases in levels of portal venous LPS suggestive of increased intestinal barrier function in AAA-10-treated rats compared to vehicle-treated animals (**Figure 5F**). Furthermore, we observed normalization of ZO-1 localization and expression, suggesting that AAA-10 treatment prevented the development of intestinal permeability in CDAHFD-fed rats (**Figure 5G**).

As intestinal permeability has been linked to translocation of intestinal products that further exacerbate hepatic inflammation[39], we performed another experiment in which we evaluated the impact of 8 day AAA-10 treatment on liver phenotypes (**Figure 6A**). Mild weight loss was observed in the AAA-10-treated animals (**Figure S10A**), consistent with our previous report that genetic removal of bacterial BSH causes altered metabolic phenotypes including reduced weight gain on a high fat diet[38]. We did not observe significant weight loss in AAA-10-treated rats in the 7 day experiment (**Figure S9B**), and we observed similar changes in ZO-1 localization and expression

in both experiments (**Figure 5G, Figure S10B**), suggesting that AAA-10-mediated protection against intestinal permeability occurred independent of weight loss. We also assessed the effect of AAA-10 or vehicle treatment on normal chow-fed rats and found no significant differences between the groups in liver or kidney function, body weight, or caloric intake (**Figure S11**), suggesting that AAA-10 itself was non-toxic and that differences between groups are directly related to changes in intestinal BA composition.

We observed dramatic histologic improvements in AAA-10-treated rats with regard to hepatic steatosis, lobular inflammation, and hepatocyte ballooning (**Figure 6B,C**). Consistent with these results, we observed significant decreases in serum measures of hepatic inflammation including ALT, AST, and alkaline phosphatase (**Figure 6D**). Finally, we observed decreased expression of pro-inflammatory and pro-fibrotic genes in treated rats (**Figure 6E-F**). Together, our findings demonstrate that treatment with the gut-restricted BSH inhibitor AAA-10 prevents the development of intestinal barrier dysfunction in CDAHFD-fed rats and leads to improved histologic features of NAFLD/NASH.

Discussion

In this study, we demonstrate that intestinal permeability is an early hallmark of a diet-induced animal model of NAFLD/NASH and that its development is associated with decreased intestinal conjugated BA concentration. Furthermore, we demonstrate a mechanism by which conjugated BAs protect the intestinal epithelial barrier from damage *in vitro* via the sequestration of unconjugated BAs in mixed micelles. Importantly, we demonstrate that increased bacterial BSH activity drives the decrease in intestinal conjugated BA concentration *in vivo*. Finally, we demonstrate that inhibition of BSH activity prevents the development of intestinal barrier dysfunction and leads to improvement in liver inflammation in CDAHFD-fed rats.

Intestinal barrier function has been implicated in the pathogenesis of a variety of metabolic diseases, including NAFLD/NASH, but the molecular mechanisms that trigger intestinal permeability defects are incompletely defined[22]. One of the key insights from our study is the importance of conjugated BAs in the maintenance of intestinal barrier function. It is known that hydrophilic BAs, including conjugated BAs, protect against cytotoxicity induced by hydrophobic bile acids, including many unconjugated species[40-42]. However, prior to our work, the mechanism of this protection remained unclear. While it was known that conjugated BAs exhibit lower CMCs than unconjugated BAs, the connection between the efficiency of mixed micelle formation by conjugated BAs and their ability to protect against unconjugated BA-induced epithelial damage had not been established. Here, we demonstrate that conjugated BAs form mixed micelles with unconjugated BAs at physiologically relevant concentrations *in vitro*. Mixed micelle formation leads to sequestration of hydrophobic, unconjugated BAs away from epithelial cells and prevents cell death and tight junction dysfunction. These data demonstrate that distinct classes of BAs elicit differential effects on intestinal epithelial permeability and delineate a mechanism by which one of these classes, conjugated BAs, protects against epithelial damage.

Another key finding from our study is the demonstration of increased bacterial BSH activity in the intestine of CDAHFD-fed rats, providing a direct mechanistic explanation for reduced conjugated BAs observed in the cecal contents of these animals. Alterations in BSH activity have previously been shown to have significant influence on directing local and systemic expression of genes involved in host metabolism[38, 43]. Interestingly, germ-free mice, which lack BSH and therefore are expected to have high levels of intestinal conjugated BAs, are resistant to development of hepatic steatosis[43]. Moreover, colonization of germ-free mice with bacteria with BSH activity induces hepatic steatosis, a phenotype that can be rescued by deletion of BSH[38].

In our model, we demonstrate that BSH activity may play an important role in the regulation of the intestinal barrier by regulating the relative concentrations of conjugated to unconjugated BA pools. Treatment of CDAHFD-fed rats with a gut-restricted BSH inhibitor allowed us to selectively modulate BA pools by increasing the abundance of intestinal conjugated BAs, a change that led not only to improvement in intestinal permeability but also reduced hepatic inflammation. The improvement in hepatic inflammation is likely multifactorial, from decreased translocation of bacterial products such as LPS as well as mild weight loss, which is likely related to metabolic changes related to BSH-dependent BA pool changes as we have previously reported[38]. Our results here demonstrate that shifting the *in vivo* BA pool to enrich for conjugated BAs prevents the development of hepatic features of NAFLD/NASH.

Overall, our findings link changes in the intestinal BA pool, specifically conjugated BAs, with maintenance of the intestinal epithelial barrier *in vivo*. Moreover, while existing studies characterizing gut dysbiosis in NAFLD/NASH have been largely descriptive, our findings highlight BSH as a critical bacterial enzyme that regulates metabolites that control gut barrier integrity. Moreover, this work provides a potential mechanistic link between changes in the microbiome and the development of metabolic diseases such as NAFLD/NASH. Our findings suggest that

strategies to shift the *in vivo* BA pool toward conjugated BAs, either by direct administration or manipulating the microbiome to reduce BSH activity, could be developed as a novel paradigm for the treatment of NAFLD/NASH.

Figure/Table Legends

Figure 1. CDAHFD-fed rats developed increased intestinal permeability before development of hepatic injury. (A) CDAHFD-fed rats developed progressive hepatic inflammation and fibrosis as demonstrated by increased alanine aminotransferase (ALT), aspartate aminotransferase (AST), alkaline phosphatase, and hepatic hydroxyproline from livers of control and CDAHFD-fed rats. n=8 per group for 48h and 1w timepoints, n=12 per group for 6w and 12w timepoints, one-way ANOVA followed by Tukey's multiple comparison test. (B) Portal venous levels of lipopolysaccharide (LPS) were significantly increased in CDAHFD-fed rats compared to control rats after 1 week on diet. n=4 per group, two-tailed Welch's t test. (C) CDAHFD diet induced intestinal inflammation. Representative hematoxylin and eosin (H&E) staining of ileum from control and CDAHFD-fed rats with pathology scores. n=8 per group, Mann-Whitney test. (D) CDAHFD induced increased expression and apical membrane localization of ZO-1 at early timepoints. ZO-1 immunofluorescence staining of ileum from control and CDAHFD-fed rats at indicated timepoints. Quantification of ZO-1 and DAPI staining intensity in ileal epithelial cells of control and CDAHFD-fed rats performed as in Supplementary Information. Intestines from all animals were stained, n=10 intestinal cell images per group were analyzed. For ZO-1 intensity, one-way ANOVA followed by Tukey's multiple comparison test, for %ZO-1 membrane intensity and DAPI intensity, two-tailed Welch's t test. (E) CDAHFD-fed rats developed evidence of increased intestinal permeability after 48 hours of diet. Measurement of FITC-Dextran levels in systemic circulation after gavage in control and CDAHFD-fed rats. n=8 per group, two-tailed Welch's t test. (F) Histologic evidence of hepatic inflammation was evident after 1 week of CDAHFD but not after 48 hours. Representative H&E staining of liver tissue from control and CDAHFD-fed rats at indicated timepoints. (G, H) Expression of pro-inflammatory and fibrosis genes were increased after 1 week of CDAHFD but not after 48 hours. Hepatic *Col1a1* and *TNFα* gene expression determined by qPCR in control and CDAHFD-fed rats at indicated timepoints. n=8 per group, two-tailed Welch's t test. *p<0.05, **p<0.005, ***p<0.001, ****p<0.0001. Bars

represent mean ± standard error of the mean (SEM).

Figure 2. BA profiles from CDAHFD-fed rats and humans with biopsy-proven NAFLD/NASH. (A-D) UPLC-MS BA analysis of portal venous serum from control and CDAHFD-fed rats after 6 and 12 weeks of diet. n=12 per group, two-tailed Welch's t test. (A, B) Total (A) and unconjugated (B) cecal BA concentrations were significantly reduced in CDAHFD-fed rats at timepoints when advanced fibrosis had developed. (C, D) Total (C) and unconjugated (D) portal venous BA concentration were significantly increased in CDAHFD-fed rats at timepoints when advanced fibrosis had developed. (E, F) Changes in fecal BA profiles in NAFLD/NASH patients with early (F0-F2; n=47) vs. advanced (F3-F4; n=15) fibrosis mirrored changes in cecal BA profiles in CDAHFD-fed rats. Student's t test. (G, H) Conjugated BAs were reduced at early timepoints in the cecum of CDAHFD-fed rats. UPLC-MS BA analysis of cecal contents from control and CDAHFD-fed rats after 48 hours and 1 week of diet. %Conjugated BA (Conjugated BAs / Total BAs * 100) are shown. n=8 per group, two-tailed Welch's t test. *p<0.05, **p<0.005, ***p<0.001, ****p<0.0001. Bars represent mean ± SEM.

Figure 3. Conjugated BAs protected epithelial monolayers from unconjugated BA-induced permeability.

(A) Cecal extracts from CDAHFD-fed rats at early timepoints caused increased epithelial permeability. Caco2 monolayer permeability after exposure to purified cecal extracts from control and CDAHFD-fed rats at indicated timepoints as measured by FITC-Dextran passage into the basolateral chamber of the transwell over 12 hours, n=3 per group, one-way ANOVA followed by Dunnett's multiple comparison test for treatment vs. DMSO, one-way ANOVA followed by Tukey's multiple comparison test for comparing treatments. (B) Unconjugated BAs increased epithelial permeability at concentrations found in the cecum of CDAHFD rats. Conjugated BAs alone did not increase permeability, and when combined with unconjugated BAs, conjugated BAs protected

against unconjugated BA-induced permeability. Caco2 monolayer permeability after exposure to indicated BA pools from control and CDAHFD-fed rats at indicated timepoints, n=3 per group, one-way ANOVA followed by Dunnett's multiple comparison test for treatment vs. DMSO, one-way ANOVA followed by Tukey's multiple comparison test for comparing treatments. (C) Schematic of *in vitro* permeability experiment. Predominant unconjugated, conjugated, and combined BA pools were added to the apical chamber of transwell system containing Caco2 monolayer and incubated for 12 hours before addition of FITC-Dextran 4kDa and fluorescence measurement from basolateral chamber. (D) Conjugated BAs protected against unconjugated BA-induced epithelial permeability at physiologic concentrations. Caco2 monolayer permeability after exposure to concentrations of BA pools as indicated. n=6 per group, 2-way ANOVA followed by Sidak's multiple comparisons test. (E) Conjugated BAs protected epithelial monolayers from unconjugated BA-induced cell death. Cell viability of Caco2 cells measured by MTT assay with BA pools at indicated concentrations. n=6 per group, 2-way ANOVA followed by Sidak's multiple comparisons test. (F) Conjugated BAs protected the physical integrity of epithelial monolayers from unconjugated BA-induced damage. Light microscopy images of H&E-stained Caco2 monolayers after exposure to BA pools at indicated concentrations. Scale bar=20 μm. (G) Conjugated BAs prevented the development of unconjugated BA-induced tight junction dilatation. TEM images of Caco2 cells from transwells after exposure to BA pools at indicated concentrations. The white arrow points to tight junction dilatation. Scale bar=500 nm. Unless otherwise specified, all experiments were performed in triplicate. *p<0.05, **p<0.005, ***p<0.001, ****p<0.0001. Bars represent mean ± SEM.

Figure 4. Conjugated and unconjugated BAs formed mixed micelles that sequester unconjugated BAs to prevent epithelial damage.

(A) Conjugated and unconjugated BAs combined exhibited a lower CMC than unconjugated BAs alone. BAs were mixed in equimolar concentrations to form BA pools. (B) Micelle formation was

disrupted after addition of urea. CMC determination for a mixture of unconjugated BAs and conjugated BAs (equimolar) and 80 mM urea. (C) TEM images of micelles formed from BA pools at indicated concentrations. Scale bar=50 nm. (D) Urea did not impact Caco2 cell viability. MTT cell viability assay of Caco2 cells in the presence or absence of 80 mM urea. (E) Micelle formation was necessary for the protective effect of conjugated BAs on epithelial permeability. Permeability measured by fluorescence (FITC-Dextran) in basolateral chamber of the transwell in the presence or absence of urea. n=6 per group, 2-way ANOVA followed by Sidak's multiple comparisons test. (F) Micelle formation was necessary for the protective effect of conjugated BAs on cell viability. Caco2 cell viability measured by MTT assay in the presence or absence of urea. n=6 per group, 2-way ANOVA followed by Sidak's multiple comparisons test. (G) Micelle formation was necessary for the protective effect of conjugated BAs on epithelial layer integrity. Light microscopy images of H&E-stained Caco2 monolayers in transwells in the presence or absence of urea. (H) Addition of urea to a mixed BA pool led to increased unconjugated BA passage across a Caco2 monolayer. Quantification of basolateral concentrations of unconjugated BAs by UPLC-MS, 2-way ANOVA followed by Sidak's multiple comparisons test. *p<0.05, **p<0.005, ***p<0.005, ****p<0.0001. Unless otherwise specified, all experiments were performed in triplicate. Bars represent mean ± SEM.

Figure 5. BSH inhibition increased intestinal conjugated BAs and restored intestinal barrier function in CDAHFD-fed rats. (A) Cecal BSH activity was increased in CDAHFD-fed rats. Cecal BSH activity of control and CDAHFD-fed rats (n=4 per group) at 48 hours of diet as measured by conversion of deuterated glyco-CDCA (GCDCA-D4) to deuterated CDCA (CDCA-D4), two-tailed Welch's t test. (B) Schematic of experimental plan for AAA-10 treatment of CDAHFD-fed rats. (C) UPLC-MS analysis of cecal contents of vehicle and AAA-10 treated (10 mg/kg twice daily) animals. n=8 per group. (D) Cecal BSH activity was reduced after 1 week of AAA-10 treatment. n=8 per group, two-tailed Welch's t-test. (E) Cecal conjugated BAs were increased in AAA-10

629 treated rats after 1 week of treatment. n=8 per group, two-tailed Welch's t test. (F) Portal venous
630 LPS levels were reduced in AAA-10 treated rats. n=8 per group, two-tailed Welch's t test. (G)
631 AAA-10 treatment prevented aberrant ZO-1 subcellular localization. ZO-1 immunofluorescence
632 and DAPI counterstaining of rat ileum with quantification from vehicle and AAA-10 treated
633 CDAHFD-fed rats at indicated timepoints. Intestines from all animals were stained, n=10 intestinal
634 cell images per group were analyzed. For ZO-1 intensity, one-way ANOVA followed by Tukey's
635 multiple comparison test, for %ZO-1 membrane intensity and DAPI intensity, two-tailed Welch's t
636 test. *p<0.05, **p<0.005, ***p<0.005, ****p<0.0001. Bars represent mean ± SEM.
637
638 **Figure 6. BSH inhibition improved hepatic inflammation in CDAHFD-fed rats.**
639 (A) Schematic of experimental design and analysis of liver-related endpoints. For (A-F), n=10 in
640 vehicle group, n=9 in AAA-10 group. (B) AAA-10 treatment prevented development of hepatic
641 steatosis and inflammation in CDAHFD-fed rats. Representative H&E staining of liver tissue from
642 vehicle or AAA-10 treated CDAHFD-fed rats. (C-D) AAA-10 treatment prevented development of
643 hepatic inflammation. (C) Histologic scoring of steatosis, hepatocyte ballooning, and lobular
644 inflammation in vehicle and AAA-10 treated animals. Mann-Whitney test. (D) Serum ALT, AST,
645 alkaline phosphatase from vehicle and AAA-10 treated rats, two-tailed Welch's t test. (E, F) AAA-
646 10 treatment attenuated hepatic gene expression of pro-inflammatory and pro-fibrotic genes in
647 CDAHFD-fed rats. RT-qPCR analysis of indicated genes in vehicle and AAA-10 treated CDAHFD-
648 fed rats, two-tailed Welch's t test. *p<0.05, **p<0.005, ***p<0.0005, ****p<0.0001. Bars represent
649 mean ± SEM.
650
651 **Table 1. Baseline characteristics of 62 patients with biopsy-proven NAFLD/NASH analyzed**
652 **in this study.** p value refers to comparison by between F0/F2 and F3-F4 fibrosis groups. Welch's
653 t test for continuous variables, chi-squared test for dichotomous variables. p < 0.05 considered
654 significant.

655 **References**

656 1. Tripathi A, Debelius J, Brenner DA, et al. The gut-liver axis and the intersection with the
657 microbiome. Nat Rev Gastroenterol Hepatol 2018;15:397-411.
658 2. Aron-Wisnewsky J, Vigliotti C, Witjes J, et al. Gut microbiota and human NAFLD:
659 disentangling microbial signatures from metabolic disorders. Nat Rev Gastroenterol
660 Hepatol 2020;17:279-297.
661 3. Boursier J, Mueller O, Barret M, et al. The severity of nonalcoholic fatty liver disease is
662 associated with gut dysbiosis and shift in the metabolic function of the gut microbiota.
663 Hepatology 2016;63:764-75.
664 4. Loomba R, Seguritan V, Li W, et al. Gut Microbiome-Based Metagenomic Signature for
665 Non-invasive Detection of Advanced Fibrosis in Human Nonalcoholic Fatty Liver
666 Disease. Cell Metab 2019;30:607.
667 5. Luther J, Garber JJ, Khalili H, et al. Hepatic Injury in Nonalcoholic Steatohepatitis
668 Contributes to Altered Intestinal Permeability. Cell Mol Gastroenterol Hepatol
669 2015;1:222-232.
670 6. Miele L, Valenza V, La Torre G, et al. Increased intestinal permeability and tight junction
671 alterations in nonalcoholic fatty liver disease. Hepatology 2009;49:1877-87.
672 7. Rahman K, Desai C, Iyer SS, et al. Loss of Junctional Adhesion Molecule A Promotes
673 Severe Steatohepatitis in Mice on a Diet High in Saturated Fat, Fructose, and
674 Cholesterol. Gastroenterology 2016;151:733-746 e12.
675 8. Mouries J, Brescia P, Silvestri A, et al. Microbiota-driven gut vascular barrier disruption
676 is a prerequisite for non-alcoholic steatohepatitis development. Journal of Hepatology
677 2019;71:1216-1228.
678 9. Buckley A, Turner JR. Cell Biology of Tight Junction Barrier Regulation and Mucosal
679 Disease. Cold Spring Harb Perspect Biol 2018;10.

10. Seki E, De Minicis S, Osterreicher CH, et al. TLR4 enhances TGF-beta signaling and hepatic fibrosis. Nat Med 2007;13:1324-32.

11. Albillos A, de Gottardi A, Rescigno M. The gut-liver axis in liver disease: Pathophysiological basis for therapy. J Hepatol 2020;72:558-577.

12. **Mouzaki M**, **Wang AY**, Bandsma R, et al. Bile Acids and Dysbiosis in Non-Alcoholic Fatty Liver Disease. PLoS One 2016;11:e0151829.

13. Nimer N, Choucair I, Wang Z, et al. Bile acids profile, histopathological indices and genetic variants for non-alcoholic fatty liver disease progression. Metabolism 2020;116:154457.

14. Puri P, Daita K, Joyce A, et al. The presence and severity of nonalcoholic steatohepatitis is associated with specific changes in circulating bile acids. Hepatology 2018;67:534-548.

15. Ridlon JM, Harris SC, Bhowmik S, et al. Consequences of bile salt biotransformations by intestinal bacteria. Gut Microbes 2016;7:22-39.

16. Foley MH, O'Flaherty S, Barrangou R, et al. Bile salt hydrolases: Gatekeepers of bile acid metabolism and host-microbiome crosstalk in the gastrointestinal tract. PLoS Pathog 2019;15:e1007581.

17. **Song Z**, **Cai Y**, Lao X, et al. Taxonomic profiling and populational patterns of bacterial bile salt hydrolase (BSH) genes based on worldwide human gut microbiome. Microbiome 2019;7:9.

18. Raimondi F, Santoro P, Barone MV, et al. Bile acids modulate tight junction structure and barrier function of Caco-2 monolayers via EGFR activation. Am J Physiol Gastrointest Liver Physiol 2008;294:G906-13.

19. Sarathy J, Detloff SJ, Ao M, et al. The Yin and Yang of bile acid action on tight junctions in a model colonic epithelium. Physiol Rep 2017;5:e13294.

20. Stenman LK, Holma R, Korpela R. High-fat-induced intestinal permeability dysfunction associated with altered fecal bile acids. World J Gastroenterol 2012;18:923-9.

21. Stenman LK, Holma R, Eggert A, et al. A novel mechanism for gut barrier dysfunction by dietary fat: epithelial disruption by hydrophobic bile acids. Am J Physiol Gastrointest Liver Physiol 2013;304:G227-34.

22. Gupta B, Liu Y, Chopyk DM, et al. Western diet-induced increase in colonic bile acids compromises epithelial barrier in nonalcoholic steatohepatitis. FASEB J 2020;34:7089-7102.

23. **Chaudhari SN**, **Harris DA**, Aliakbarian H, et al. Bariatric surgery reveals a gut-restricted TGR5 agonist with anti-diabetic effects. Nat Chem Biol 2021;17:20-29.

24. Fluksman A, Benny O. A robust method for critical micelle concentration determination using coumarin-6 as a fluorescent probe. Anal Methods 2019;11:3810-3818.

25. Adhikari AA, Seegar TCM, Ficarro SB, et al. Development of a covalent inhibitor of gut bacterial bile salt hydrolases. Nat Chem Biol 2020;16:318-326.

26. Matsumoto M, Hada N, Sakamaki Y, et al. An improved mouse model that rapidly develops fibrosis in non-alcoholic steatohepatitis. Int J Exp Pathol 2013;94:93-103.

27. Chaudhari SN, Luo JN, Harris DA, et al. A microbial metabolite remodels the gut-liver axis following bariatric surgery. Cell Host Microbe 2021;29:408-424.

28. Guo W, Wang P, Liu ZH, et al. Analysis of differential expression of tight junction proteins in cultured oral epithelial cells altered by Porphyromonas gingivalis, Porphyromonas gingivalis lipopolysaccharide, and extracellular adenosine triphosphate. Int J Oral Sci 2018;10:e8.

29. Guan Y, Watson AJ, Marchiando AM, et al. Redistribution of the tight junction protein ZO-1 during physiological shedding of mouse intestinal epithelial cells. Am J Physiol Cell Physiol 2011;300:C1404-14.

30. Odenwald MA, Choi W, Buckley A, et al. ZO-1 interactions with F-actin and occludin direct epithelial polarization and single lumen specification in 3D culture. J Cell Sci 2017;130:243-259.

31. **Hagstrom H**, **Nasr P**, Ekstedt M, et al. Fibrosis stage but not NASH predicts mortality and time to development of severe liver disease in biopsy-proven NAFLD. J Hepatol 2017;67:1265-1273.

32. Arab JP, Karpen SJ, Dawson PA, et al. Bile acids and nonalcoholic fatty liver disease: Molecular insights and therapeutic perspectives. Hepatology 2017;65:350-362.

33. **Li F**, **Jiang C**, Krausz KW, et al. Microbiome remodelling leads to inhibition of intestinal farnesoid X receptor signalling and decreased obesity. Nat Commun 2013;4:2384.

34. Soderholm JD, Olaison G, Peterson KH, et al. Augmented increase in tight junction permeability by luminal stimuli in the non-inflamed ileum of Crohn's disease. Gut 2002;50:307-13.

35. Hofmann AF. The Function of Bile Salts in Fat Absorption. The Solvent Properties of Dilute Micellar Solutions of Conjugated Bile Salts. Biochem J 1963;89:57-68.

36. Pavlovic N, Golocorbin-Kon S, Ethanic M, et al. Bile Acids and Their Derivatives as Potential Modifiers of Drug Release and Pharmacokinetic Profiles. Front Pharmacol 2018;9:1283.

37. Adhikari AA, Ramachandran, D., Chaudhari, S. N., Powell, C. E., McCurry, M.D., Banks, A.S., Devlin, A.S. A gut-restricted lithocholic acid analog as an inhibitor of gut bacterial salt hydrolases. bioRxiv 2021. https://www.biorxiv.org/content/10.1101/2021.03.15.435552v1

38. Yao L, Seaton SC, Ndousse-Fetter S, et al. A selective gut bacterial bile salt hydrolase alters host metabolism. Elife 2018;7.

39. Chopyk DM, Grakoui A. Contribution of the Intestinal Microbiome and Gut Barrier to Hepatic Disorders. Gastroenterology 2020;159:849-863.

40. Hegyi P, Maleth J, Walters JR, et al. Guts and Gall: Bile Acids in Regulation of Intestinal Epithelial Function in Health and Disease. Physiol Rev 2018;98:1983-2023.

41. Araki Y, Andoh A, Bamba H, et al. The cytotoxicity of hydrophobic bile acids is ameliorated by more hydrophilic bile acids in intestinal cell lines IEC-6 and Caco-2. Oncol Rep 2003;10:1931-6.

42. Di Ciaula A, Wang DQ, Molina-Molina E, et al. Bile Acids and Cancer: Direct and Environmental-Dependent Effects. Ann Hepatol 2017;16 Suppl 1:S87-S105.

43. Brandl K, Schnabl B. Intestinal microbiota and nonalcoholic steatohepatitis. Curr Opin Gastroenterol 2017;33:128-133.

Author names in bold designate shared co-first authorship.

Figure 1

A

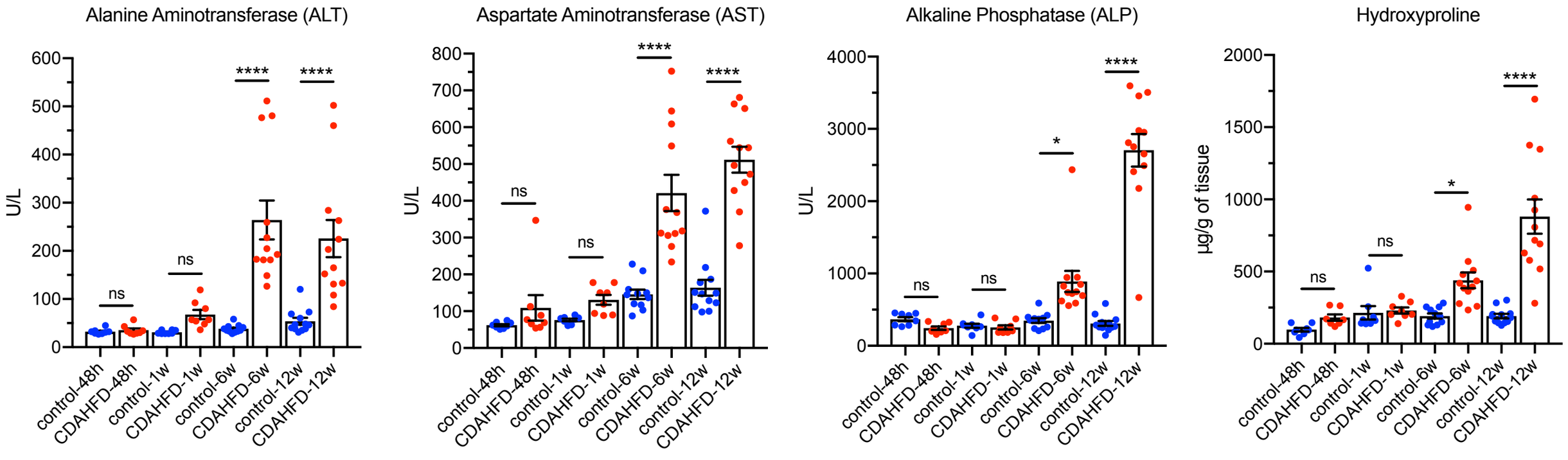

B

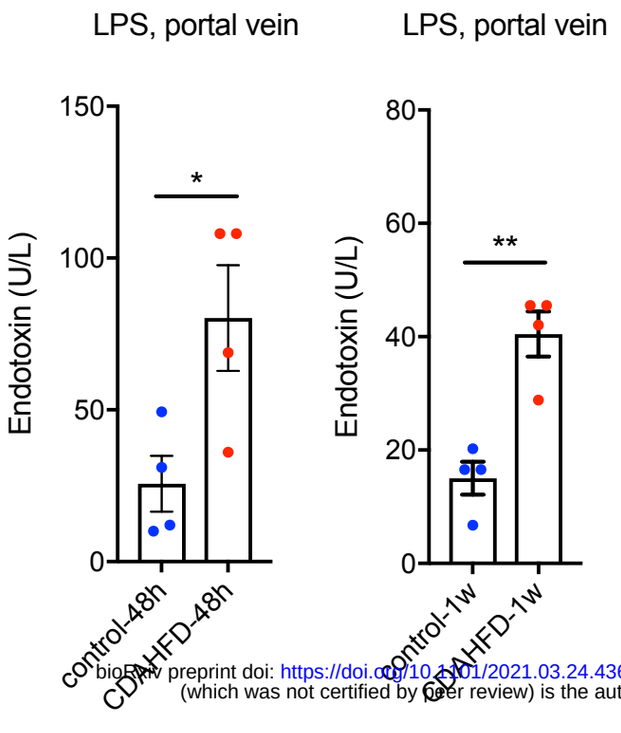

C

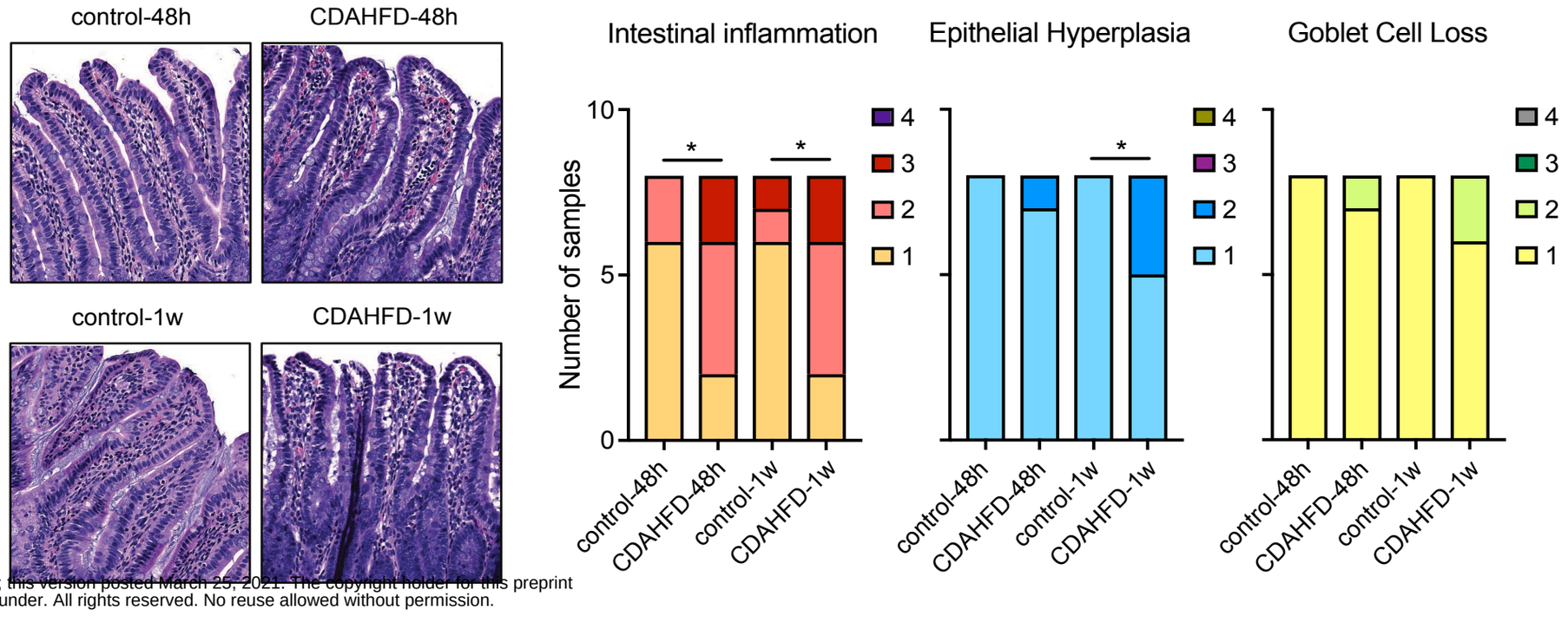

D

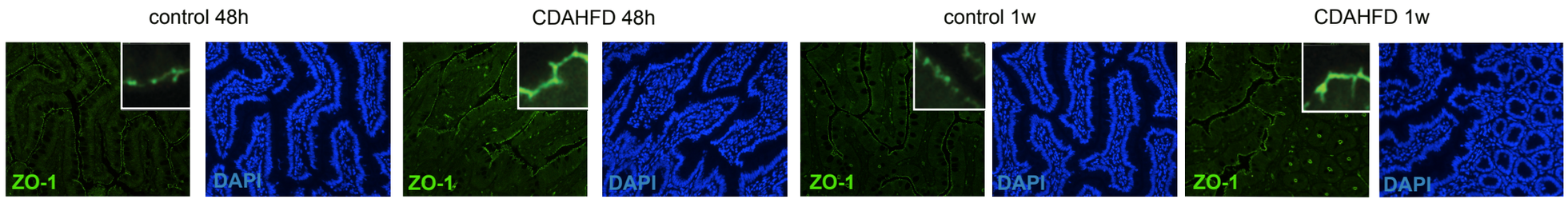

E

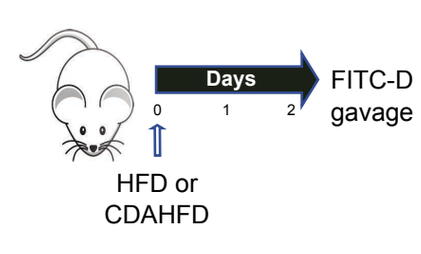

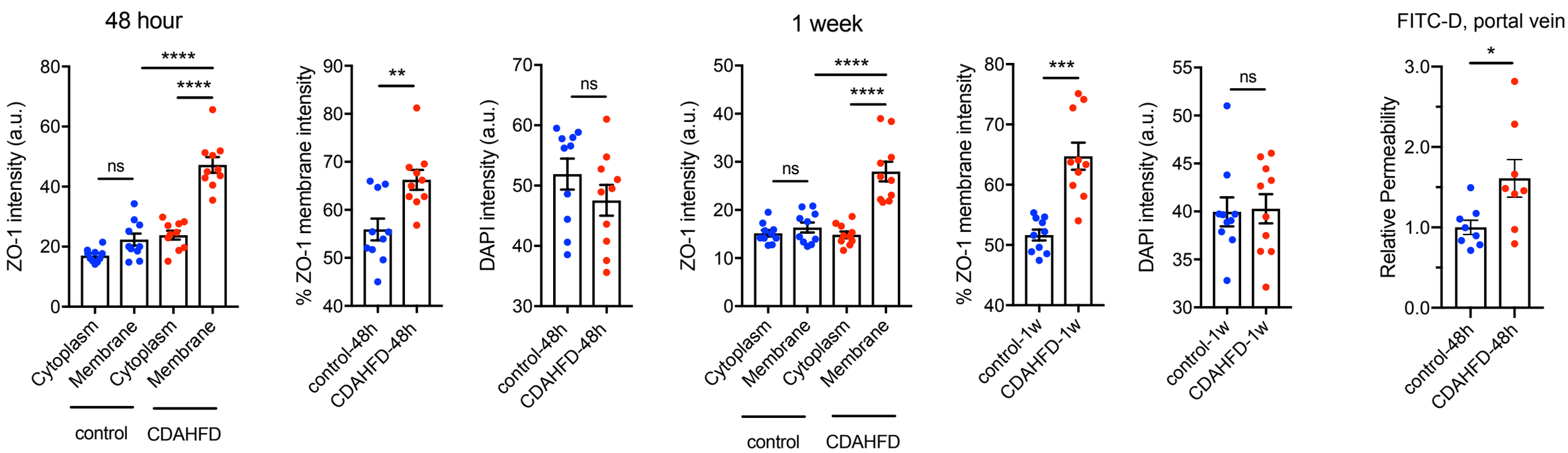

F

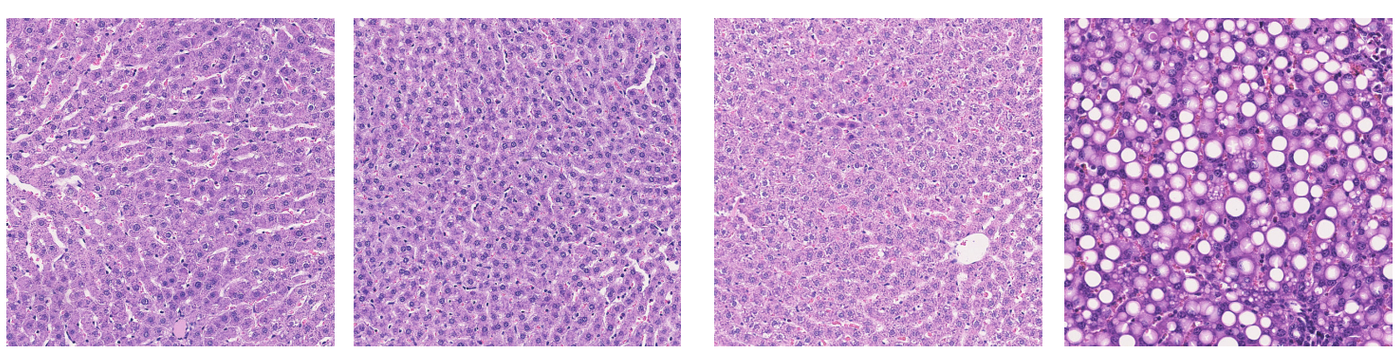

G

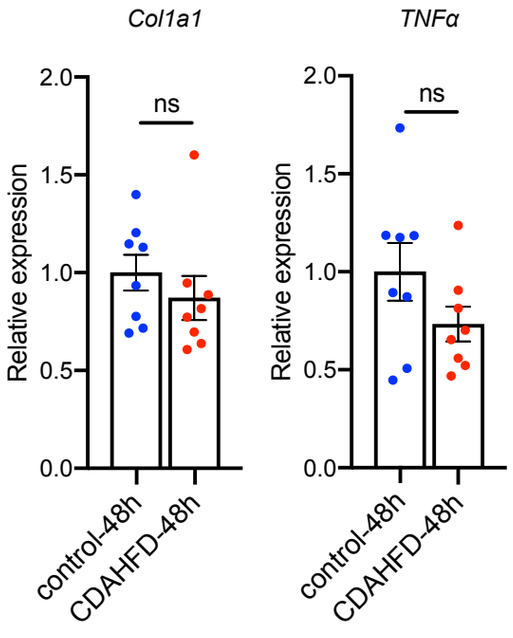

H

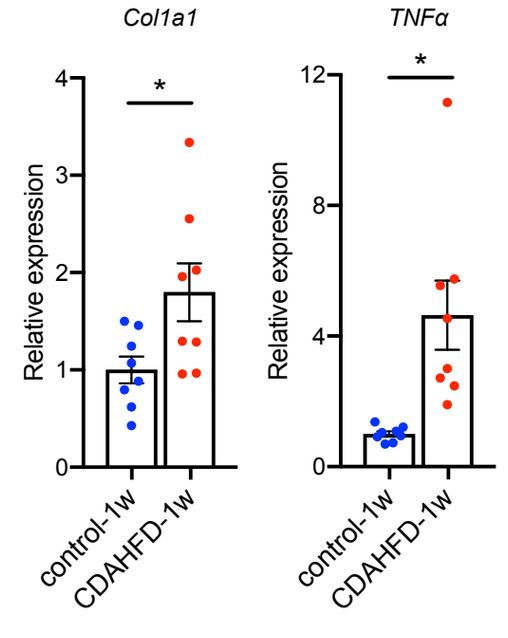

Figure 2

Figure 3

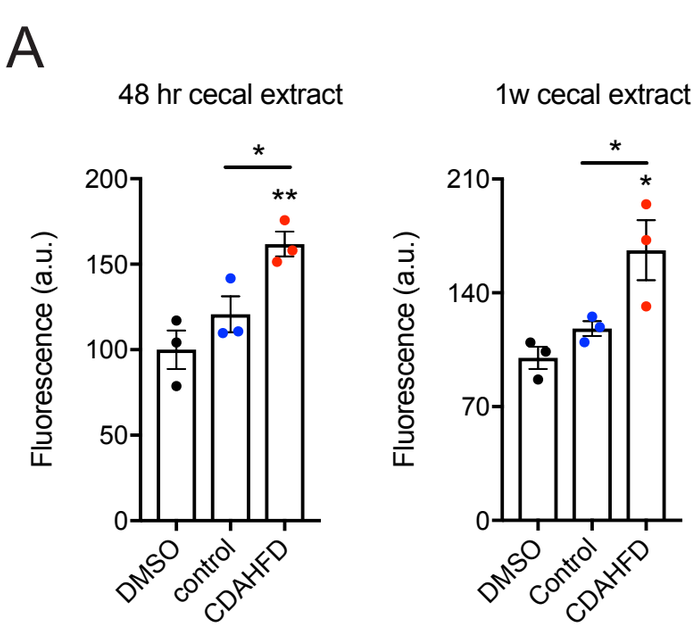

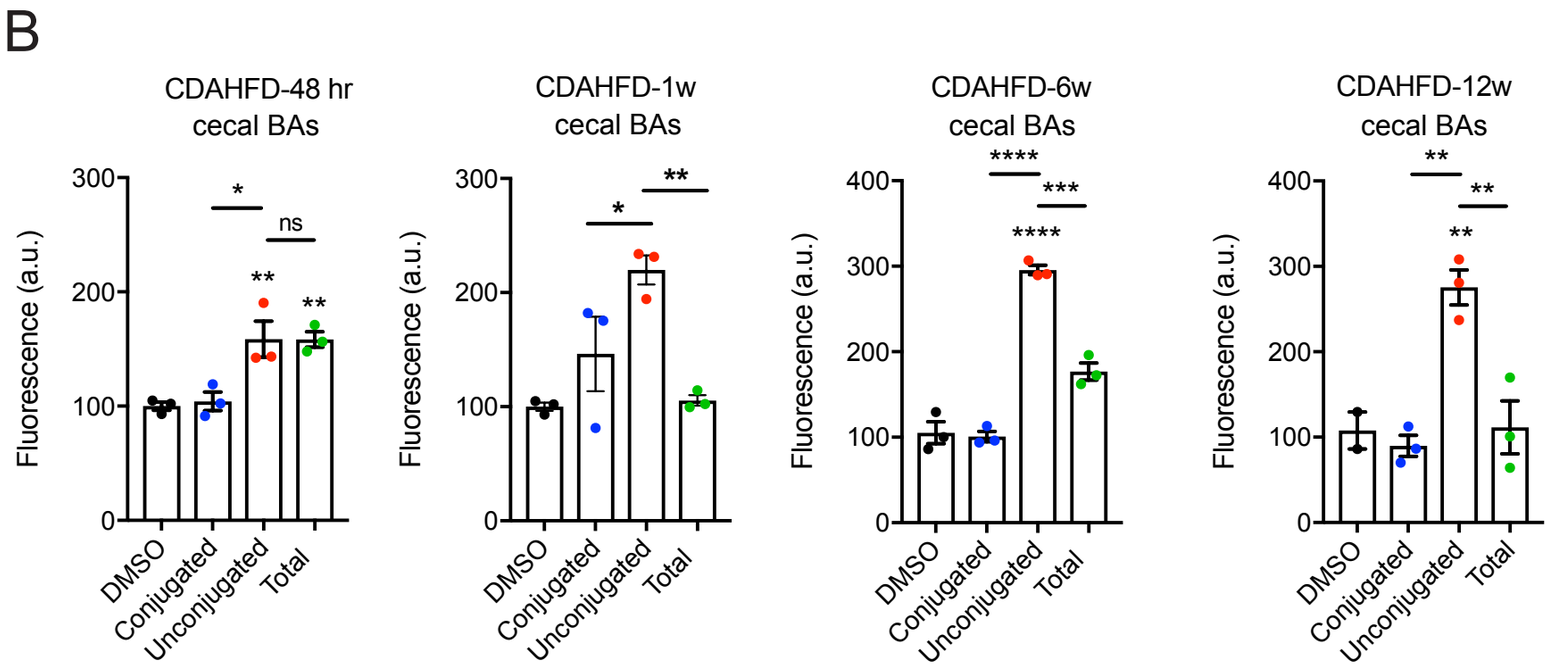

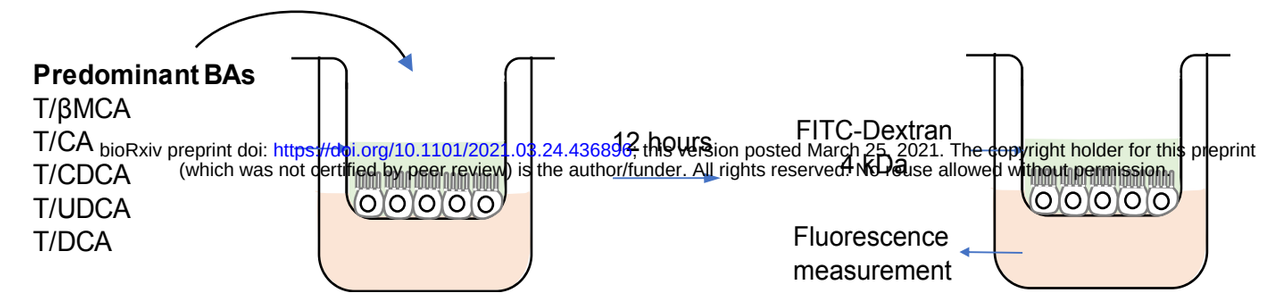

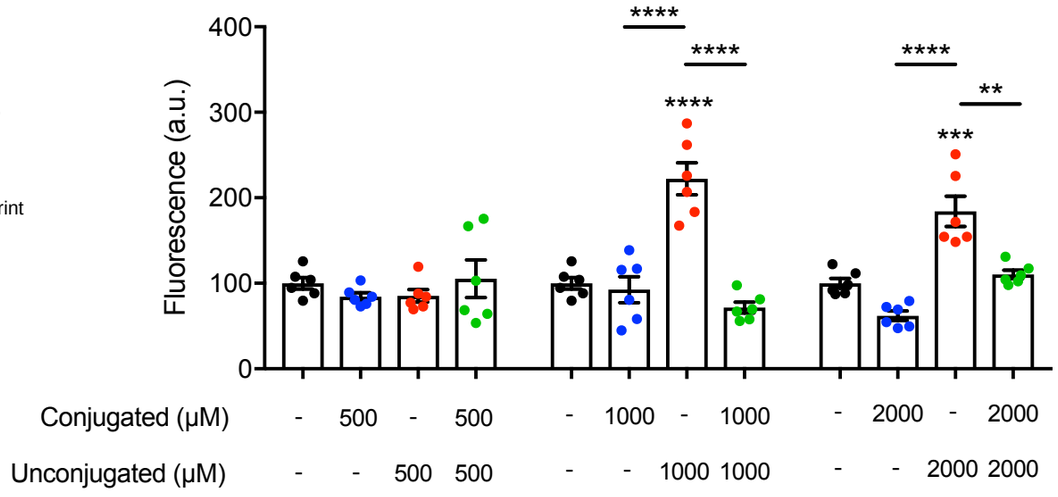

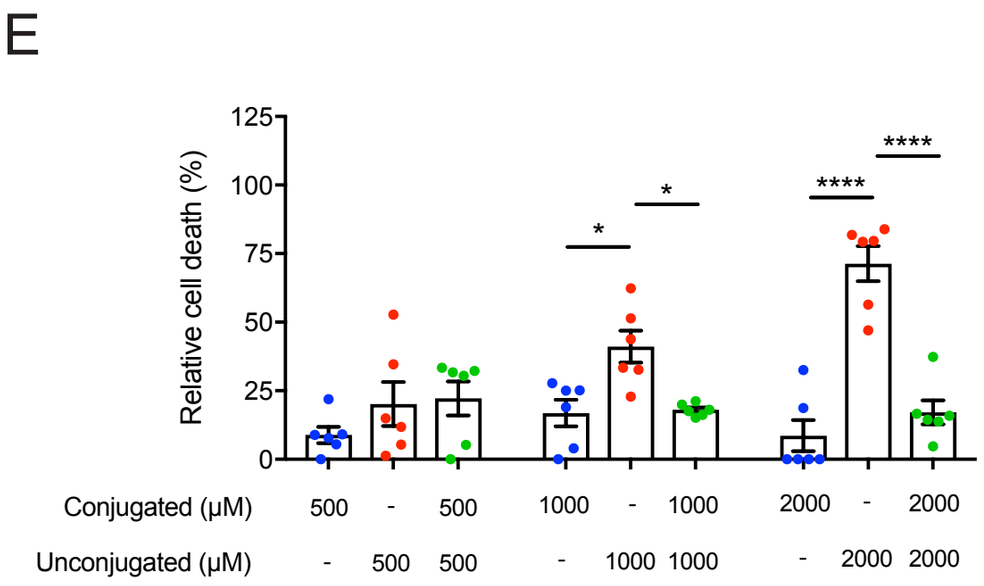

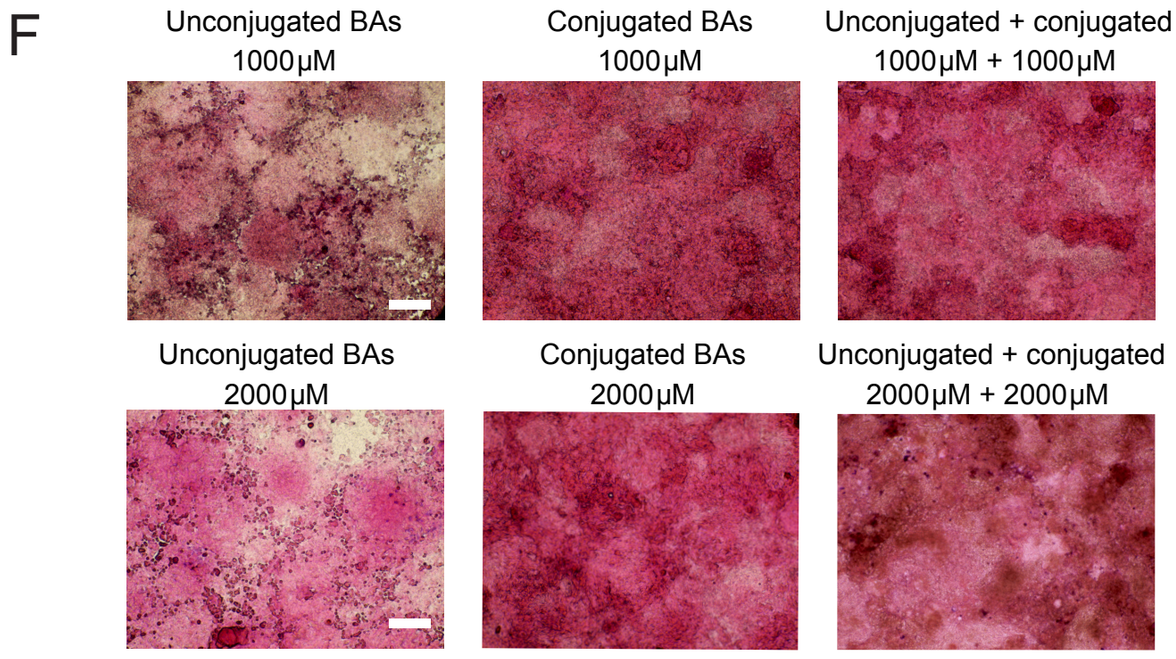

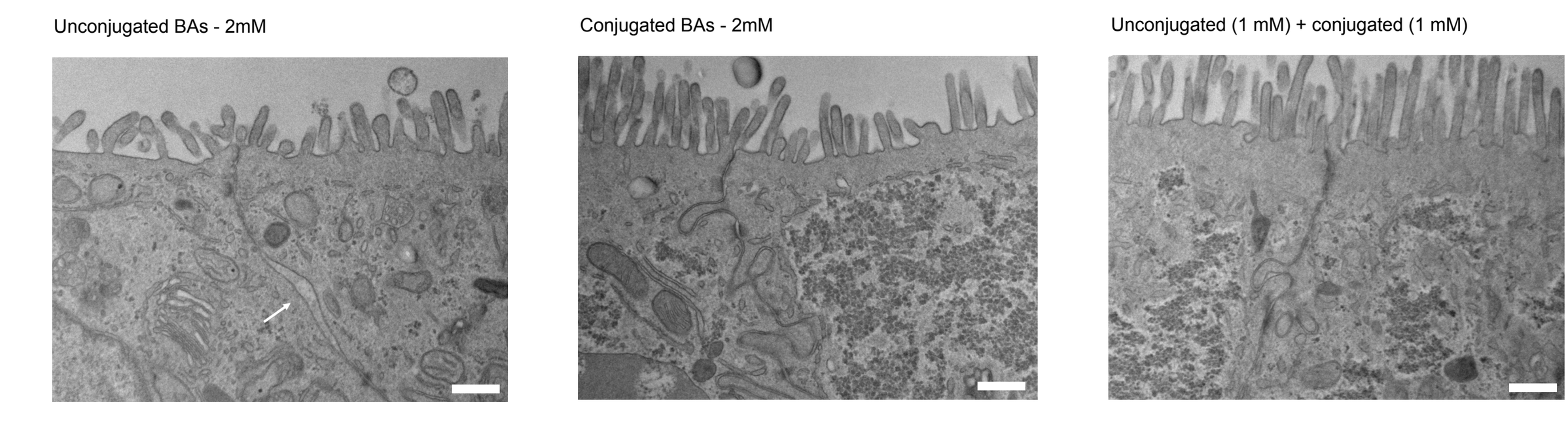

Figure 4

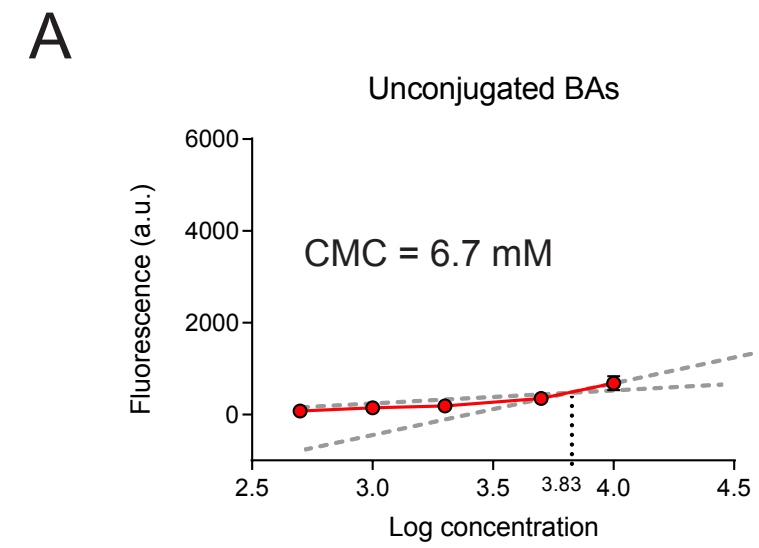

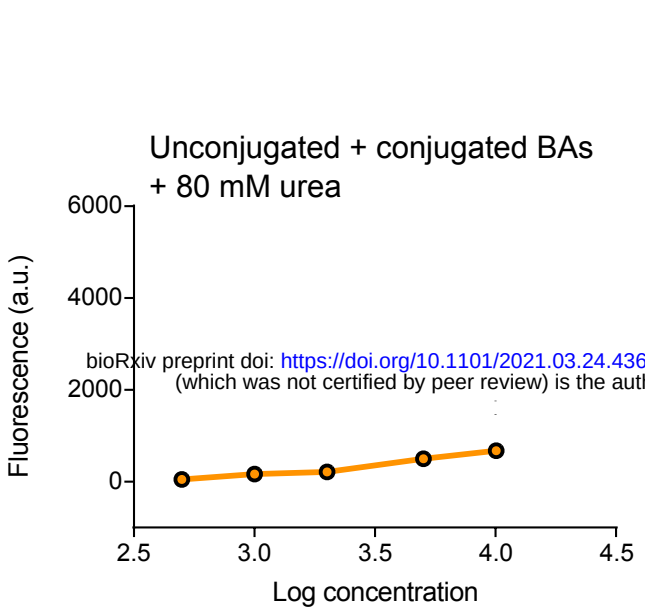

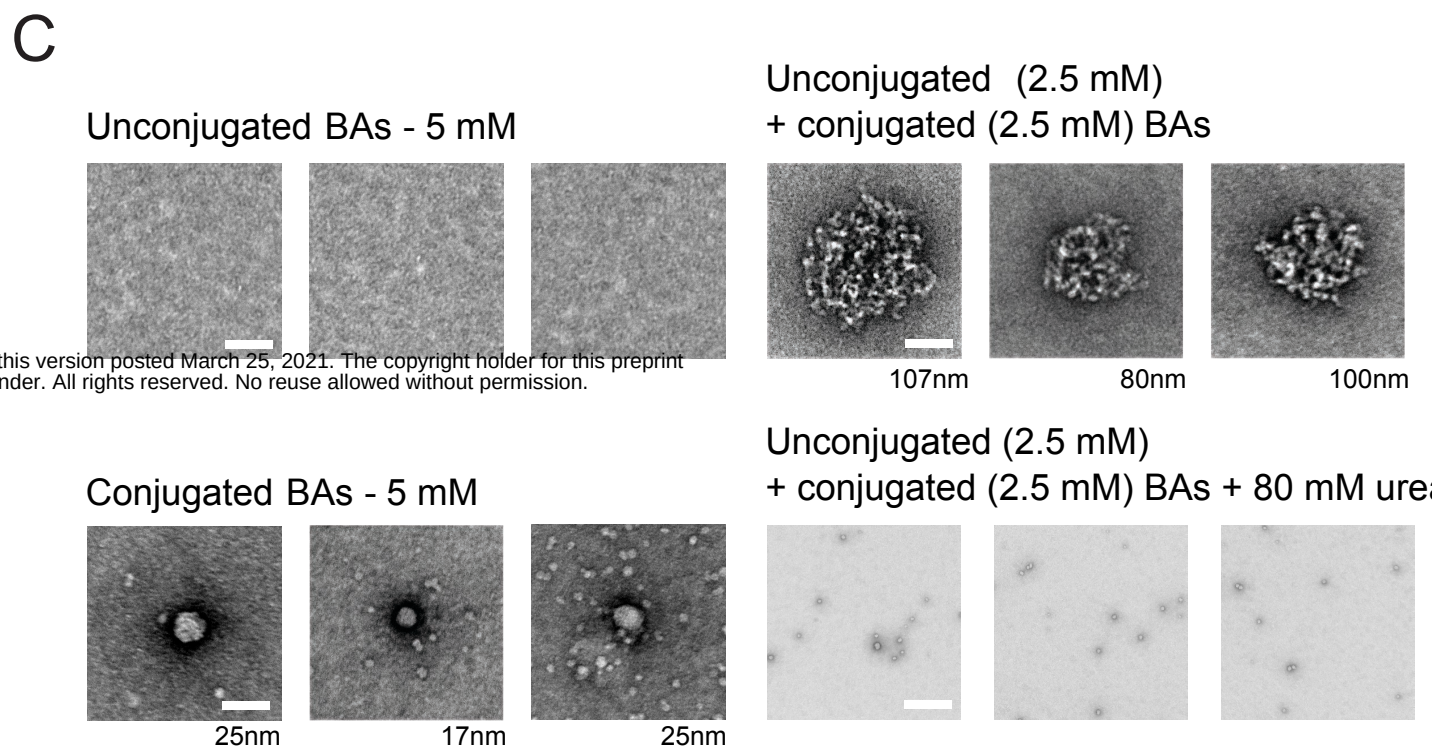

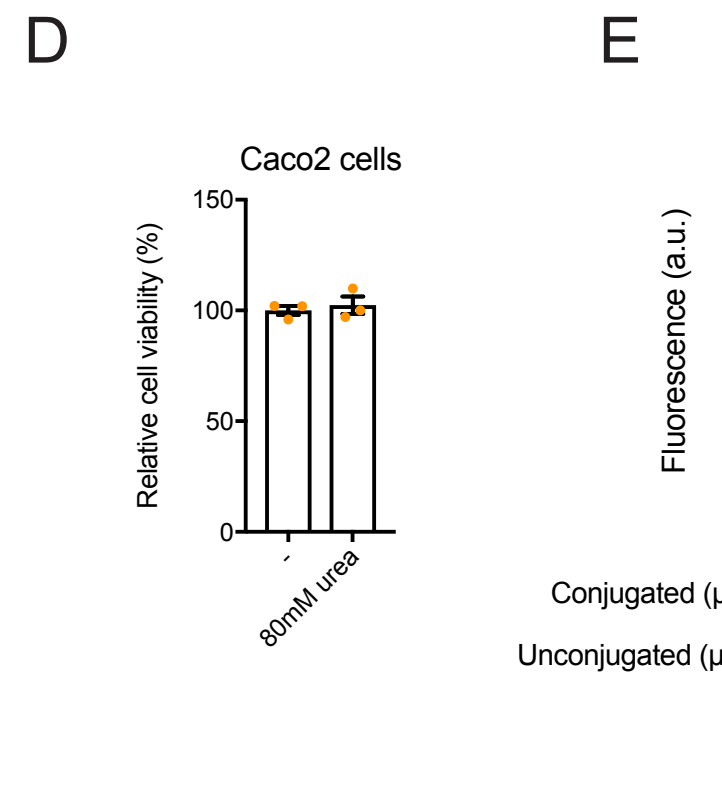

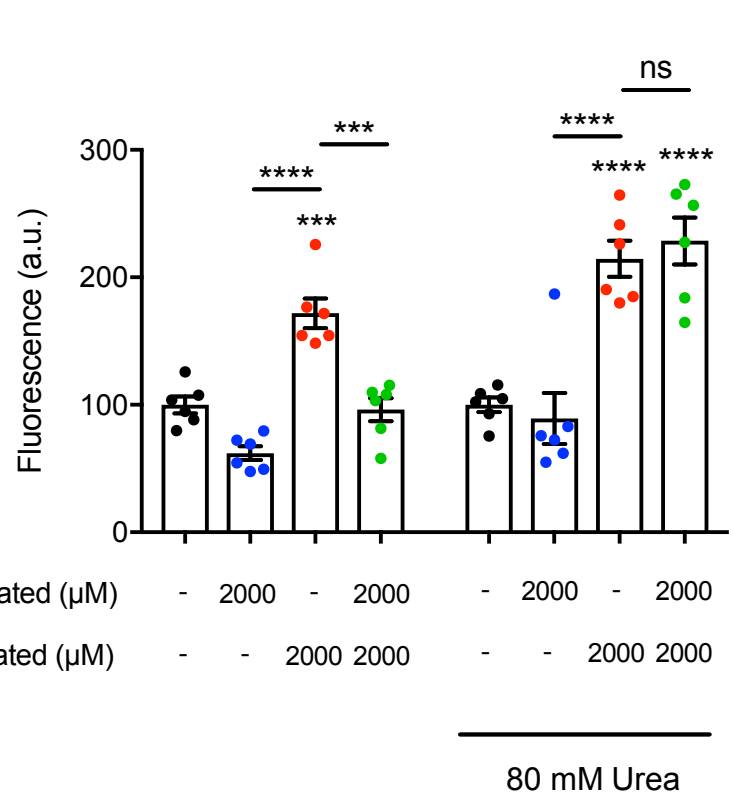

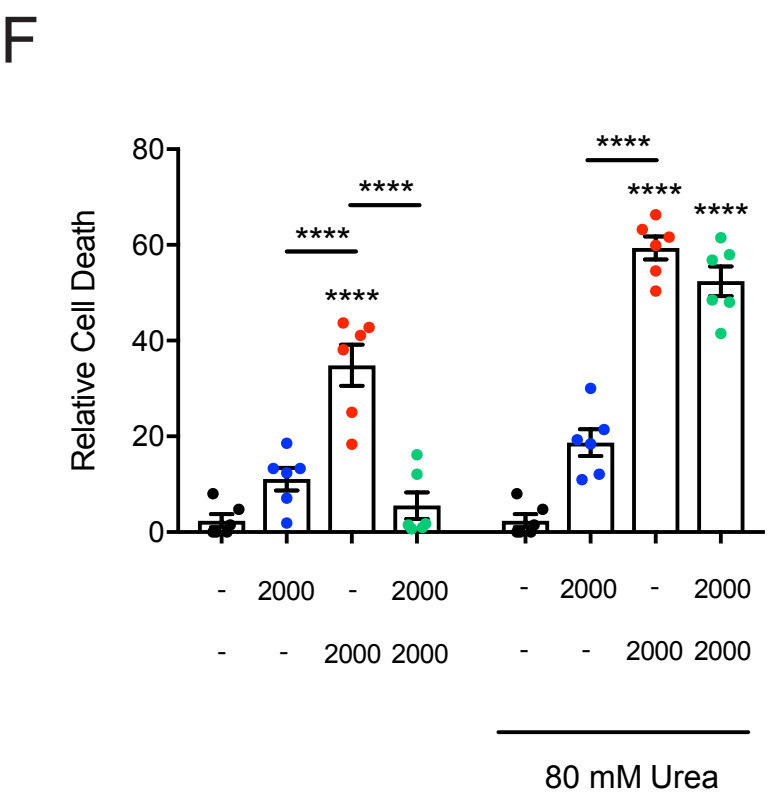

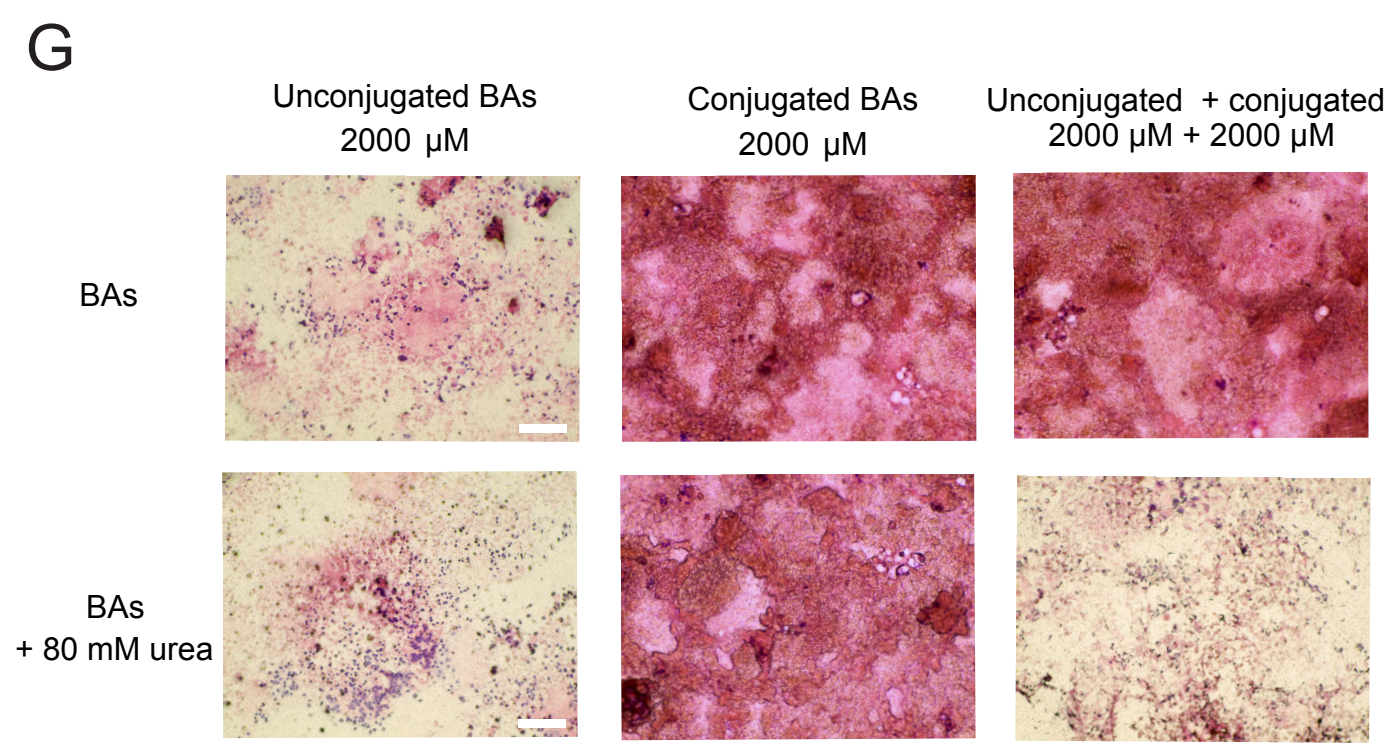

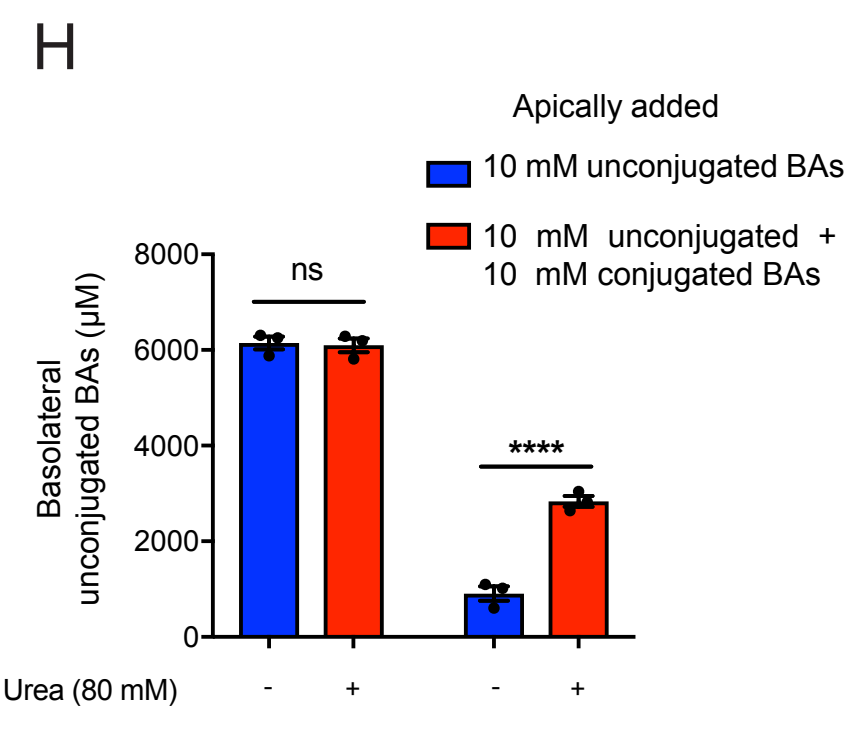

Figure 5

A

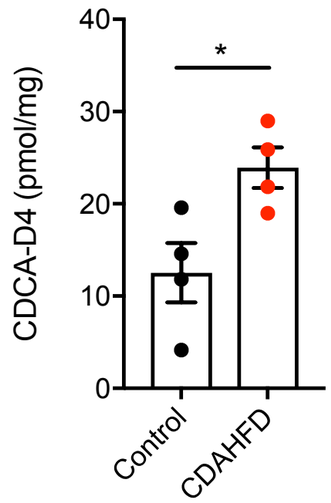

B

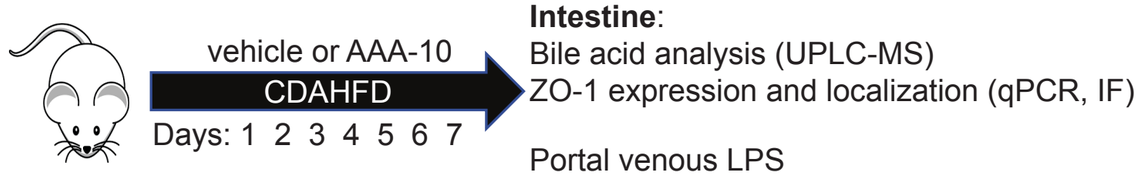

C

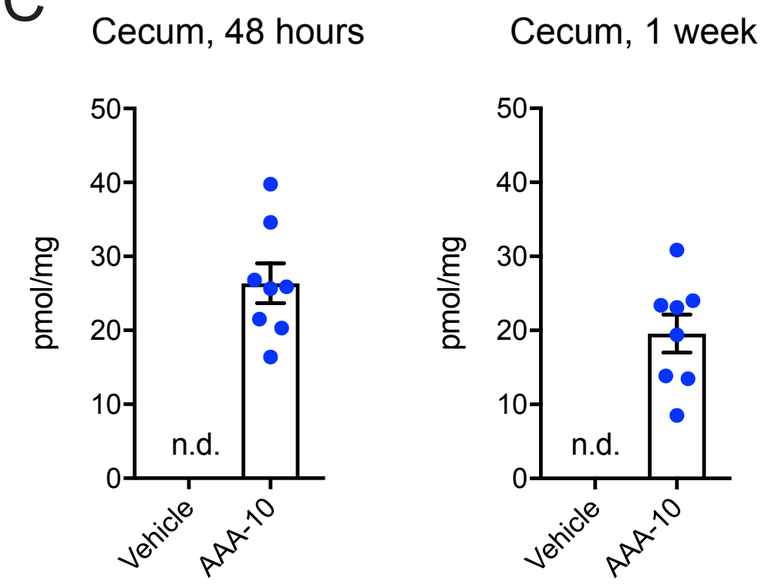

D

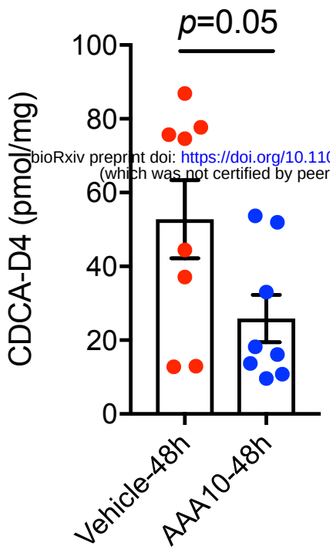

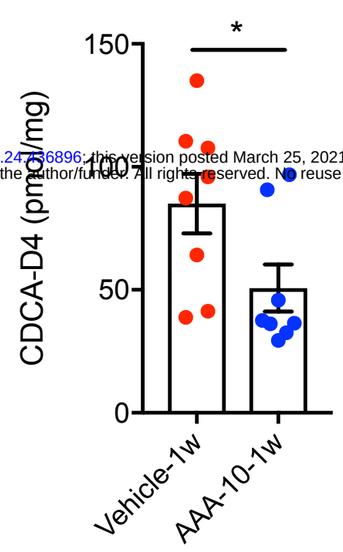

E

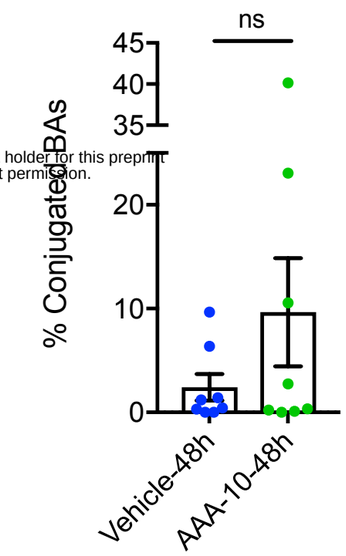

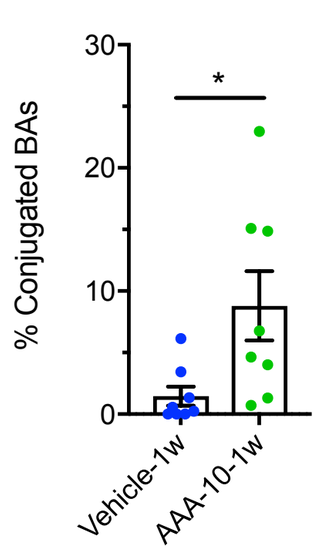

F

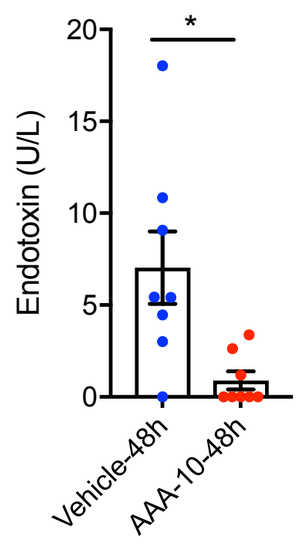

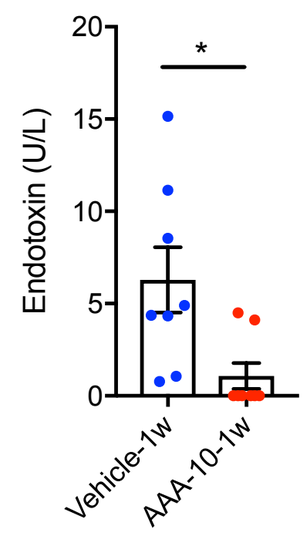

G

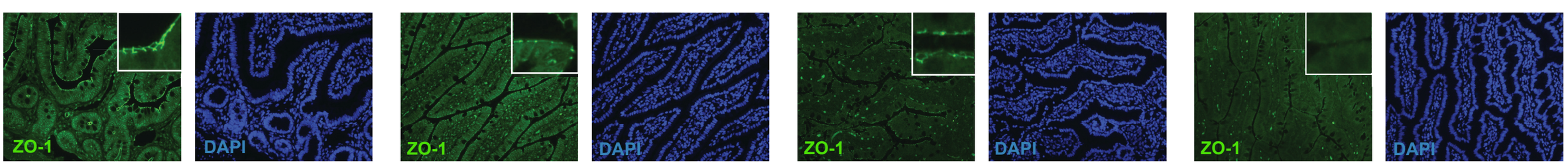

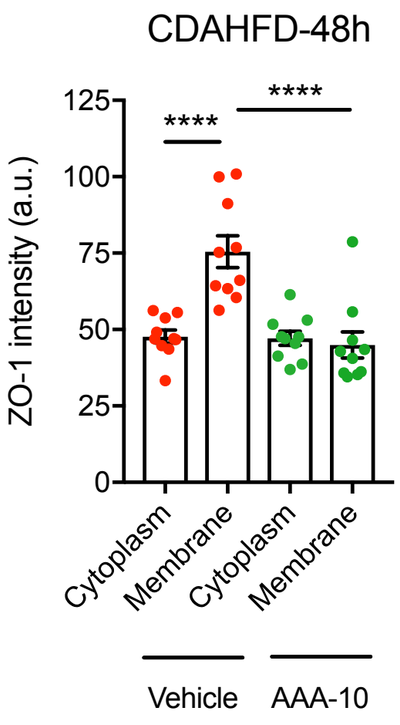

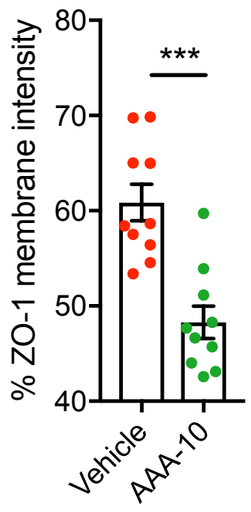

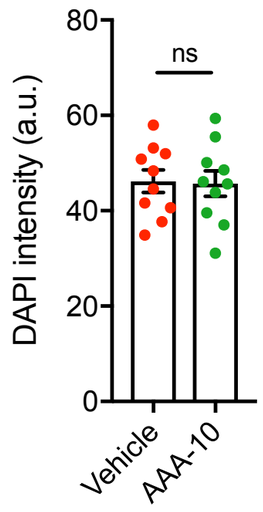

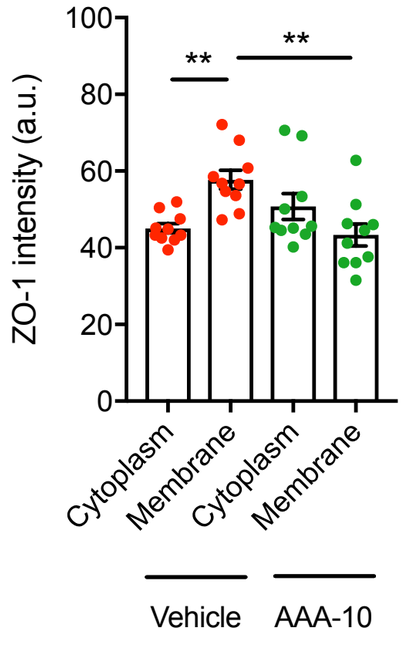

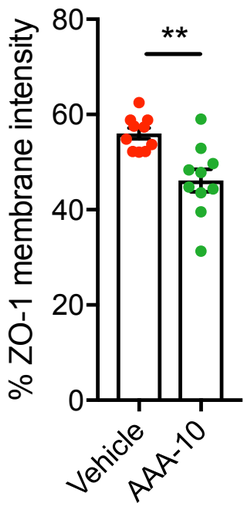

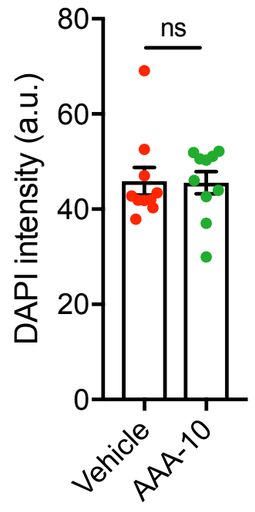

A

B

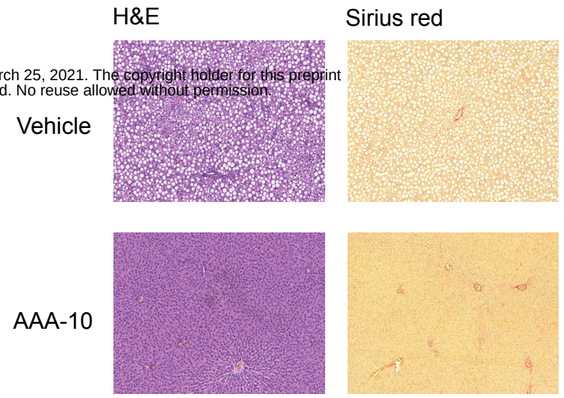

C

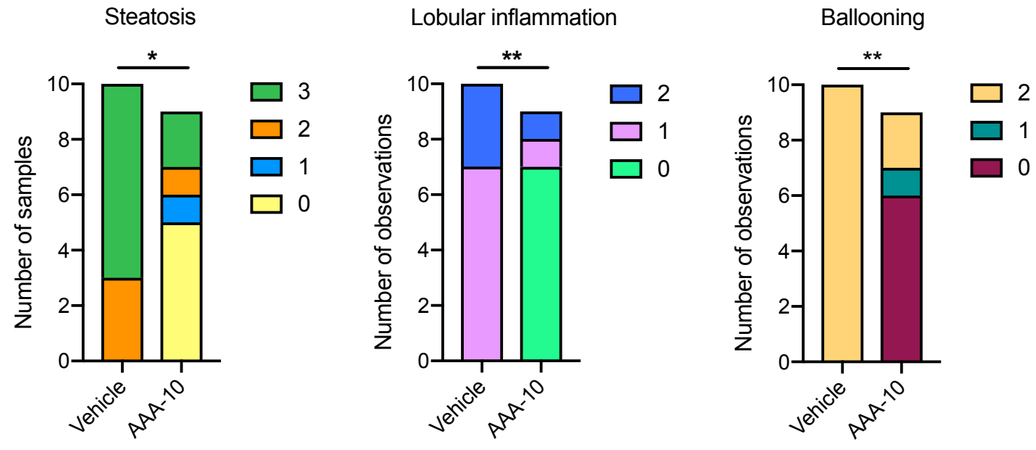

D

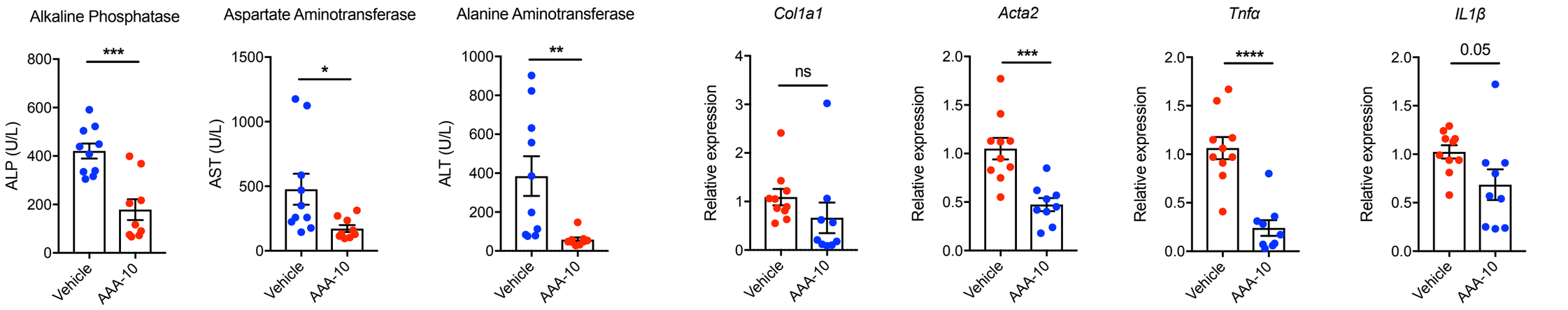

E

F